Ocean Engineering 334 (2025) 121613

Contents lists available at ScienceDirect

Ocean Engineering

journal homepage: www.elsevier.com/locate/oceaneng

Research paper

Stabilizing dynamic subsea power cables using Bi-stable nonlinear energy sinks

Anargyros Michaloliakos [a,*], Wei-Ying Wong [b], Ryan Davies [c], Malakonda Reddy Lekkala [c], Matthew Hall [c], Lei Zuo [b], Alexander F. Vakakis [a]

[a] Department of Mechanical Science and Engineering, University of Illinois Urbana-Champaign, USA
[b] Department of Naval Architecture and Marine Engineering, University of Michigan, Ann Arbor, USA
[c] National Renewable Energy Laboratory, Golden, CO, USA

ARTICLE INFO

Keywords:
Bi-stable nonlinear energy sink (B-NES)
Wavelet transform
Subsea power cable
Offshore wind energy
Vibration

ABSTRACT

This study investigates vibration mitigation of dynamic subsea cables through passive bi-stable nonlinear energy sinks (B-NESs). These devices suppress vibration energy in a broadband way, and can be regarded as extensions of classical linear tuned mass dampers (TMDs) which are narrowband devices. Through the open-source MoorDyn library, we simulated the vibrations of a vertical subsea cable equipped with a set of B-NESs. Multi-objective optimization was performed to detect the B-NES parameters for optimal mitigation of the cable vibrations. Advanced signal processing verified the efficacy of the optimized B-NESs not only to rapidly absorb and locally dissipate vibration energy, but also to nonlinearly scatter vibration energy from low to high frequencies within the cable itself. This last feature is especially beneficial for vibration mitigation of the undersea cable, as at higher frequencies the cable vibrations exhibit drastically reduced amplitudes and are more effectively dissipated by inherent structural damping and hydrodynamic radiation damping. This contrasts with traditional TMDs which can mitigate vibration only at a single frequency. Furthermore, our robustness study confirms the B-NES's effectiveness under even varying environmental conditions. Overall, the B-NES's capacity for broadband vibration mitigation renders it a promising retrofit solution for improving the performance and operational safety of dynamic power cables in offshore wind farms and other marine applications.

1. Introduction

The rapid deployment of offshore wind energy globally is fueled by advancements in technology, the evolution of supply chains, competitive markets, and extensive experience from large-scale projects. Notably, the U.S. government aims to escalate U.S. offshore wind capacity from under 1 GW–30 GW by 2030, highlighting the strategic expansion of the offshore wind energy sectors (N. Skopljak, 2016). Floating offshore wind turbines are critical in exploiting vast oceanic areas with rich wind resources, especially in regions where water depths exceed 60 m, rendering traditional fixed-bottom installations cost-prohibitive. About 20 % of an offshore wind farm's expenditure is tied to its electrical infrastructure, which includes costly subsea power cables essential for energy transmission from turbines to shore. However, these subsea cables, especially the dynamic cables that connect floating wind turbine platforms to the substation, face substantial risks of mechanical failures. According to Lloyd Warwick, an international insurance company, approximately 83 % of all offshore-wind-related financial losses stem from power cable issues (LLOYD Warwick, 2021). The dynamic cables are particularly vulnerable, as they are subject to continuous platform motion and environmental forces like tidal currents and waves, which induce oscillations leading to fatigue. Consequently, failures in these cables not only necessitate costly repairs but also significantly undermine the reliability and economic viability of offshore wind farms. Therefore, addressing the stability and durability of dynamic cables is crucial for enhancing the resilience and efficiency of floating offshore wind energy transmission systems.

The focus on subsea dynamic power cables is driven by their susceptibility to platform motion and dynamic environmental forces such as ocean currents and tidal flows, which impose complex loading conditions on these structures. Such conditions can potentially lead to severe structural damage or failure if not adequately mitigated. The current methods used to mitigate the effects of environmental loads on subsea cylindrical structures, such as risers and cables, involve devices

* Corresponding author.
E-mail address: am71@illinois.edu (A. Michaloliakos).

https://doi.org/10.1016/j.oceaneng.2025.121613
Received 13 December 2024; Received in revised form 6 May 2025; Accepted 18 May 2025
Available online 21 May 2025
0029-8018/© 2025 The Authors. Published by Elsevier Ltd. This is an open access article under the CC BY license (http://creativecommons.org/licenses/by/4.0/).

that alter the hydrodynamic behavior of the structures. Examples of these devices include helical strakes, streamlined fairings, and ribbons, hairs, or fringes (Drumond et al., 2018). These devices are mounted externally on the subsea cable to change the hydrodynamics and reduce vibrations in a passive way (Drumond et al., 2018). In the latest research on the performance of helical strakes in different models (continuous, serrated, and inverted), Assi et al. (2022) reported that the most efficient serrated strake reduced the peak amplitude of oscillations by 95 %, producing 54 % less drag than a bare cable in specific excitation conditions. A study on flexible risers (Quen et al., 2014), however, demonstrated that the effectiveness of helical strakes in terms of suppressing vibrations and reducing hydrodynamic forces on a flexible cylinder structure is less than that of a rigid cylinder. Another device is fairings, which have a streamlined shape that can reduce the formation of vortices that induce vibrations of the cable (Zheng and Wang, 2017). Yet, galloping oscillations have been observed in practical applications of fairings at relatively high incoming velocities. Furthermore, these hydrodynamics-based cable add-ons increase the cable size and thereby increase hydrodynamic drag loads, which can cause critical structural loading in regions with large ocean currents.

Instead of the use of hydrodynamics-based devices, another approach to reduce the mechanical vibrations is to take advantage of the mechanism of the resonance of mechanical vibrations (Frahm, 1911). Resonant mechanical vibrations pose a considerable challenge across various structural engineering domains. Particularly in scenarios where structures exhibit low inherent damping capacities, the implementation of supplementary damping devices, known as vibration absorbers, becomes essential. These devices are integral in effectively managing the vibrational energy of primary structures—often referred to as host structures. The principal mechanism behind these vibration absorbers is dynamic vibration absorption, wherein the absorber vibrates out of phase with the structure, creating a counteracting force that reduces the overall oscillation amplitude. The most common form of these devices is the tuned mass damper (TMD), which functions by attaching a mass to the host structure through a linear coupling, precisely tuned to resonate at a critical natural frequency of the host (Elias and Matsagar, 2017; Gutierrez Soto and Adeli, 2013; Hoang et al., 2008; Miranda, 2005; Ormondroyd and Den Hartog, 1928; Rana and Soong, 1998; Tsai, 1995). Although effective within narrow frequency ranges, TMDs operate optimally when the system's natural frequencies are stable. However, operational conditions often vary, leading to frequency shifts that expose the limitations of a TMD's narrow operational bandwidth; hence, the suppression performance of these devices is not robust to changing frequency or mistuning. Corrosion, variations in temperature and pressure depending on depth, and the tension of the cable are crucial parameters that create a dynamic environment and contribute to the varying operational conditions of the dynamic subsea power cable. Additionally, large displacements experienced by TMDs may lead to excessive stresses and fatigue, potentially compromising structural integrity and system performance. These challenges underscore the necessity for a new class of vibration absorbers that can be effective over a broader frequency spectrum, leading to robust suppression of non-stationary excitations, and at the same time, exhibiting relatively small oscillation amplitudes during operation.

Another inevitable challenge in the subsea environment is the biofouling effect on subsea structures. Marty et al. (2021) indicated that biofouling increases the surface roughness, weight, and size of subsea dynamic cables, thereby altering their dynamic behavior. This change is characterized by modified drag and inertia properties, which can compromise the effectiveness of traditional hydrodynamic devices designed to operate under specific environmental conditions. Additionally, the increased mass attributable to biofouling can alter the natural frequency of subsea cables. This shift is particularly problematic for TMDs, as their effectives relies on matching the natural frequency of the structures they are designed to protect. When this frequency deviates from the TMD's optimal range, the efficacy of the damping mechanism diminishes, increasing the risk of structural failure.

In response to these limitations, and to specifically address the challenges associated with subsea dynamic power cables in marine environments, this paper explores the innovative application of nonlinear energy sinks (NESs), which are passive, lightweight, dissipative local attachments with inherent strong nonlinearity. NESs are designed to absorb and dissipate vibrational energy by leveraging their nonlinearity, which enables them to adapt dynamically to varying energy levels (Gendelman et al., 2001; Gendelman, 2001; Vakakis and Gendelman, 2001). Unlike conventional TMDs, however, NESs are devoid of a fixed resonance frequency; instead, their response frequencies are tunable with energy, i.e., they adapt to (change with respect to) the frequency and energy content of the applied excitations. This is a key feature of NESs, as it allows them to dissipate energy from multiple modes of the host structure across a spectrum of energies and frequencies, which results in multi-scale targeted energy transfer. This includes engaging in complex interactions, which are pivotal in ensuring that NESs remain effective over a broad range of energy conditions (Gendelman et al., 2001; Gendelman, 2001; Starosvetsky and Gendelman, 2010; Vakakis et al., 2009, 2022; Vakakis and Gendelman, 2001). This characteristic makes NESs particularly suited for mitigating both stationary and non-stationary vibrations across extensive frequency spectra, thereby adapting to dynamic inputs without the necessity for frequency-specific tuning. Traditional approaches to vibration mitigation, like the integration of linear devices designed to absorb or dampen these oscillations, often fall short given the unique challenges posed by the marine environment. Thus, there are exciting prospects in leveraging NESs for their capacity to manage energy transfer within these systems effectively. NESs are particularly advantageous in environments where operational conditions can vary widely and unpredictably, due to their ability to adapt to a range of dynamic inputs without the need for tuning to specific frequencies (Quinn et al., 2011).

The use of NESs for passive mitigation of large-amplitude structural vibrations has proven effective across various applications, such as suppressing aeroelastic instabilities in aircraft wings (Gendelman et al., 2010), mitigating blast and seismic events (Gzal et al., 2024; Nucera et al., 2010; Wierschem et al., 2013), and providing acoustic isolation and non-reciprocity (Bellet et al., 2010; Michaloliakos et al., 2023). Additionally, an NES can be integrated with energy-harvesting elements such as piezoelectric (Nili Ahmadabadi and Khadem, 2014; Zhang et al., 2017), magnetostrictive (Fang et al., 2017), or electromagnetic (Kremer and Liu, 2014; Mann and Sims, 2009; Remick et al., 2016) systems to capture vibration energy from the structure via the targeted energy transfer (TET) mechanism. Recent studies have experimentally and numerically explored both linear and nonlinear damping solutions for marine and offshore applications (Tian et al., 2023). Experimental investigations by (Sardar and Chakraborty, 2025). and (Wang et al., 2025) demonstrated significant vibration mitigation in marine environments using compliant liquid dampers and gyro stabilizers, respectively. However, limited work exists specifically exploring the application of NES technology for stabilizing dynamic subsea power cables in offshore wind farms.

Bi-stable NESs (B-NESs) are a special type of NES that are uniquely suited for dissipating energy over a wide frequency range, making them particularly effective in managing vibrations within complex and variable environments like those encountered by subsea dynamic power cables. The extra adaptivity of the dynamics of the B-NES is enabled by its bi-stable nature, which allows it to switch between two stable equilibrium points, facilitating a range of resonant interactions that enhance energy dissipation. Indeed, at high energy levels, the B-NES engages in strongly modulated oscillations governed by fundamental and superharmonic resonances, effectively dissipating energy through robust oscillatory motion. For lower energy inputs, the B-NES undergoes chaotic oscillations cross potential wells, as well as subharmonic resonances, which enable efficient energy transfer even under mild excitation conditions (Manevitch et al., 2014; Romeo et al., 2015). This

versatility makes the B-NES a powerful tool for mitigating impulsive or broadband excitations, providing a robust solution to extend the lifespan and improve the stability of subsea dynamic power cables subjected to time-variable marine conditions.

This paper is a first attempt to investigate the potential of using B-NES attachments to stabilize subsea dynamic power cables against environmental excitations. We present computational models to demonstrate the efficacy of B-NES systems in reducing the amplitude of oscillations from environmental interactions. By shifting the focus from traditional applications to the stabilization of subsea power cables using B-NES technology, this paper aims to highlight novel applications of this nonlinear-based technology in enhancing the resilience and functionality of critical marine structure. The paper is structured as follows: Section 2 describes the system setup and modeling methodology, including a detailed explanation of the lumped-mass model theory behind the MoorDyn simulation environment. Section 3 explains the optimization framework employed to refine the B-NESs that will be attached to the subsea cable. Utilizing high-performance computing (HPC), we explore a broad parameter space to identify the B-NES settings that maximize vibration reduction, enhancing the system's robustness in real-world conditions. Section 4 investigates the robustness of the B-NES in mitigating vibrations of dynamic subsea cables, particularly under variations in their dynamic features caused by environmental effects such as biofouling. In this section, we also incorporate stochastic excitations to reflect real-world uncertainties. Lastly, Section 5 discusses the broader implications of this study, emphasizing the potential of B-NES technology to enhance the durability and operational safety of subsea power cables. We also outline future work, including plans to incorporate vortex-induced vibration (VIV) modeling and further optimization of B-NES configurations for enhanced effectiveness.

2. System description and numerical implementation

We now present a detailed discussion of the modeling and analysis techniques used for studying the dynamics of a subsea power cable with or without the B-NES attached. We first introduce the numerical simulation framework employed, followed by the analytical and numerical approaches used to model the system's behavior. These results serve as the foundation for validating the numerical simulations and comparing them with analytical derivations to ensure accuracy and effectiveness in real-world applications.

2.1. Modeling of the subsea dynamic power cable

In this work, we used the lumped-mass mooring model MoorDyn for the simulation of the subsea dynamic power cable and the B-NES device. MoorDyn is an open-source time-domain mooring dynamics library integrated into numerous floating renewable energy simulators, including the National Renewable Energy Laboratory's floating wind turbine simulation tool OpenFAST (Hall and Goupee, 2015). MoorDyn has the capability to model rigid-body dynamics, shared mooring lines, line failures, and dynamic power cables. MoorDyn has four core objects that can be used to construct a mooring system: lines, points, rods, and bodies.

MoorDyn employs lumped-mass discretization to represent mooring lines as point masses connected by linear spring-damper segments, which allows for elasticity in the axial direction (Fig. 1). If $\boldsymbol{r_i}$ and $\boldsymbol{r_{i+1}}$ represent the absolute position vectors of two adjacent nodes, the strain $e_{i+\frac{1}{2}}$ in the segment connecting them is given as,

$$e_{i+\frac{1}{2}} = \left(\frac{|\boldsymbol{r}_{i+1} - \boldsymbol{r}_i|}{l} - 1\right) \tag{2.1.1}$$

where l is the unstretched segment length. The tangent direction at a node i is approximated as a unit vector aligned between the nodes on either side:

$$\widehat{\boldsymbol{q}}_i = \frac{\boldsymbol{r}_{i+1} - \boldsymbol{r}_{i-1}}{|\boldsymbol{r}_{i+1} - \boldsymbol{r}_{i-1}|} \tag{2.1.2}$$

The tension forces acting on each segment, denoted by $\boldsymbol{T}_{i+\frac{1}{2}}$ (due to

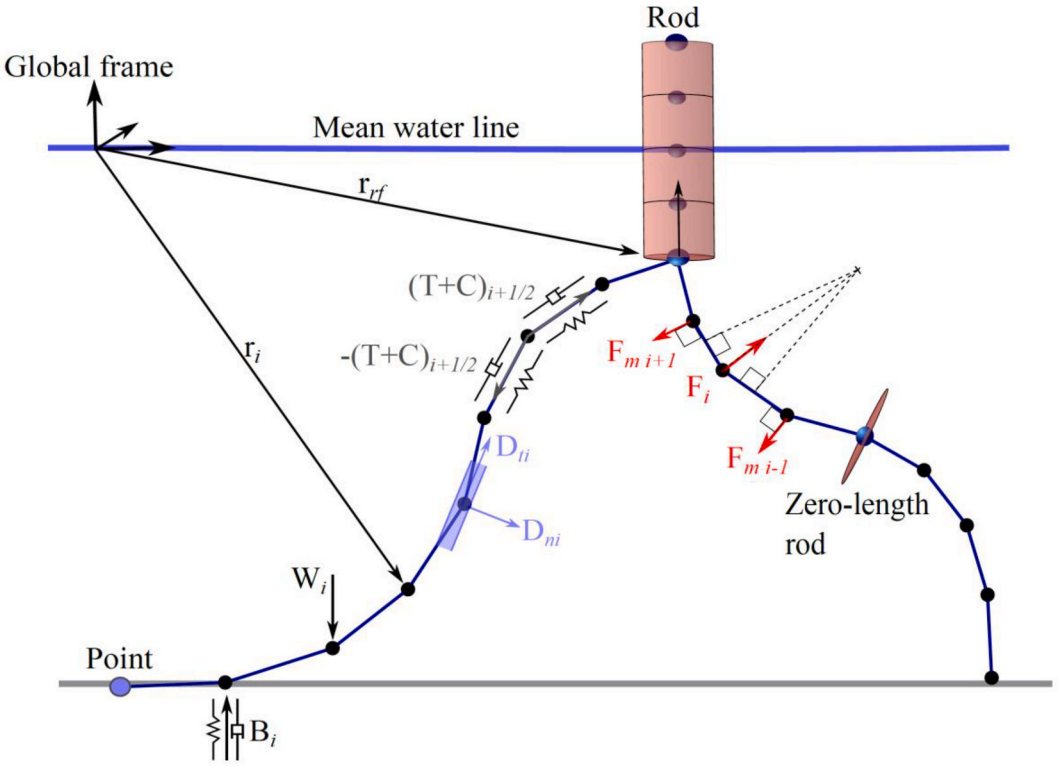

Fig. 1. Schematic of the MoorDyn lumped mass model.

material stiffness) and by $\boldsymbol{C}_{i+\frac{1}{2}}$ (due to internal damping), are then computed as,

$$\boldsymbol{T}_{i+\frac{1}{2}} = E\frac{\pi}{4}\mathrm{d}^2 e_{i+\frac{1}{2}}{}^{*}\widehat{\boldsymbol{q}}_i \tag{2.1.3}$$

$$\boldsymbol{C}_{i+\frac{1}{2}} = C_{\mathrm{int}}\frac{\pi}{4}\mathrm{d}^2\frac{\partial e_{i+\frac{1}{2}}{}^{*}}{\partial t}\,\widehat{\boldsymbol{q}}_i \tag{2.1.4}$$

where d is the line diameter, E the elasticity modulus, and C_{int} the internal damping coefficient. The strain rate of the segment, $\frac{\partial e_{i+\frac{1}{2}}}{\partial t}$, is calculated as:

$$\frac{\partial e_{i+\frac{1}{2}}}{\partial t} = \frac{\partial}{\partial t}\left(\frac{|\boldsymbol{r}_{i+1} - \boldsymbol{r}_i|}{l} - 1\right) \tag{2.1.5}$$

Structural damping is introduced to critically damp non-physical resonances arising from segment discretization. External forces are also accounted for in MoorDyn, including hydrodynamics and seabed interactions. Hydrodynamic forces such as drag and added mass are incorporated using the Morison equation. The general theory behind these is described in (Hall and Goupee, 2015). Seabed interaction theory is explained in (Housner et al., 2022).

Dynamic cables can be modeled in MoorDyn as *line objects* with a non-zero bending stiffness term. *Zero-length rods* are used as 6 degree of freedom (DOF) points to attach the cable to other objects such as other cables and bodies so that bending moments due to cable motion are properly accounted for. This method of cable modeling in MoorDyn is frequently used by users and was verified in the original cable implementation study (Hall et al., 2021). In the absence of rotational DOFs to MoorDyn's line nodes, a bending moment is implemented by applying transverse forces on the nodes, perpendicular to the axial stiffness forces. The bending moment at a given location along the line is calculated as $M = EI\kappa$, where EI is the cable's bending stiffness (the product of the elasticity modulus and cross-sectional moment of inertia) and κ is the local cable curvature. The curvature κ at node i is defined as,

$$\kappa_i = \frac{2}{dl}\sqrt{1 - \widehat{\boldsymbol{q}}_{i-\frac{1}{2}}\cdot\widehat{\boldsymbol{q}}_{i+\frac{1}{2}}} \tag{2.1.6}$$

where dl is the unstretched cable length between adjacent nodes and $\widehat{\boldsymbol{q}}_{i-\frac{1}{2}}$ and $\widehat{\boldsymbol{q}}_{i+\frac{1}{2}}$ are the unit tangent vectors between nodes. The bending moment can then be represented as a set of forces on the nodes and their neighboring nodes. Unit vector $\boldsymbol{b}_i$ is the axis of curvature at node i and can be expressed as follows:

$$\boldsymbol{b}_i = \frac{\widehat{\boldsymbol{q}}_{i-\frac{1}{2}} \times \widehat{\boldsymbol{q}}_{i+\frac{1}{2}}}{\left|\widehat{\boldsymbol{q}}_{i-\frac{1}{2}} \times \widehat{\boldsymbol{q}}_{i+\frac{1}{2}}\right|} \tag{2.1.7}$$

These forces are applied to nodes i−1 and i+1 to create the bending moment across node i, with the magnitudes given by:

$$\boldsymbol{F}_{m,i-1} = \frac{M}{dl}\cdot\left(\widehat{\boldsymbol{q}}_{i-\frac{1}{2}} \times \boldsymbol{b}_i\right) \tag{2.1.8}$$

$$\boldsymbol{F}_{m,i+1} = \frac{M}{dl}\cdot\left(\widehat{\boldsymbol{q}}_{i+\frac{1}{2}} \times \boldsymbol{b}_i\right) \tag{2.1.9}$$

Because these forces are applied to the adjacent nodes, they give rise to a non-physical net force at node i, which, in turn, is neutralized by an opposing force applied to node i:

$$\boldsymbol{F}_i = -\left(\boldsymbol{F}_{m,i-1} + \boldsymbol{F}_{m,i+1}\right) \tag{2.1.10}$$

This approach allows for bending stiffness to be included in MoorDyn line objects without any change to the line state vector or other load calculations.

The final integrated equation of motion for each node of the subsea cable, accounting for the node mass and other forces such as tension, damping, and drag, is expressed as,

$$(\boldsymbol{m}_i + \boldsymbol{a}_i)\frac{\partial^2 \boldsymbol{r}_i}{\partial t^2} = \boldsymbol{T}_{i+\frac{1}{2}} - \boldsymbol{T}_{i-\frac{1}{2}} + \boldsymbol{C}_{i+\frac{1}{2}} - \boldsymbol{C}_{i-\frac{1}{2}} + \boldsymbol{F}_i + \boldsymbol{W}_i + \boldsymbol{B}_i + \boldsymbol{D}_{ni} + \boldsymbol{D}_{ti} \tag{2.1.11}$$

where $\boldsymbol{W}_i$ is the submerged weight, $\boldsymbol{B}_i$ is the bottom contact force, and $\boldsymbol{D}_{ni}$ and $\boldsymbol{D}_{ti}$ are the normal and tangential drag forces, respectively. Lastly, $\boldsymbol{m}_i$ is defined as the 3x3 identity matrix multiplied by the mass of the node, whereas $\boldsymbol{a}_i$ is the 3 × 3 added-mass matrix. These are both described in (Hall and Goupee, 2015).

Points are 3-DOF objects used to connect lines to each other, the platform, or the seabed. They can have mass and volume, allowing them to simulate things like clump weights and floats. They follow the same kinematic theory as line nodes and have external forcing from hydrodynamics and any attached lines.

Rod objects are similar to lines in that they use a lumped-mass approach, but the masses are rigidly connected along a central axis. Hall et al. (Hall, 2020) introduced zero-length rods as a 6-DOF point object for passing bending moments from dynamic cables to their attached object. A key implementation step for rod objects is lumping the forces and masses at each node along the rod length into a single set of 6-DOF forces and mass coefficients at the rod reference point. To lump forces, the point force vectors $\boldsymbol{f}_i$ at each node i along the rod are combined into a single force and moment vector $\boldsymbol{f}_6$ at the rod reference point (end A) using,

$$\boldsymbol{f}_6 = \sum_i \begin{pmatrix} \boldsymbol{f}_i \\ \boldsymbol{f}_i((\boldsymbol{r}_i - \boldsymbol{r}_{\mathrm{rf}} \times \boldsymbol{f}_i) \end{pmatrix} \tag{2.1.12}$$

where $\boldsymbol{r}_i$ represents the global position of each node and $\boldsymbol{r}_{\mathrm{rf}}$ is the reference point for the rod.

For transforming the mass of an object to a new reference position $\boldsymbol{r}'$, the following expressions are used,

$$\boldsymbol{M}' = \sum_i \boldsymbol{M}_i \tag{2.1.13}$$

$$\boldsymbol{I}' = \sum_i \left(\boldsymbol{M}_i\boldsymbol{H}_i\boldsymbol{H}_i^T + \boldsymbol{H}_i\boldsymbol{I}_i\boldsymbol{H}_i^T + \boldsymbol{J}_i\right) \tag{2.1.14}$$

where $\mathbf{H}$ is the matrix of antisymmetric tensor components, defined as $\boldsymbol{H}_{ij} = \epsilon_{ijk}d_k$, in which $\mathbf{d} = \mathbf{r}' - \mathbf{r}$ and ϵ is the Levi-Civita (permutation) symbol.

Bodies are more general 6-DOF objects that can have rods and points attached to them. They can be used to simulate the rigid-body dynamics of a platform or attach the other objects rigidly. The dynamics of the system consider both forces and mass contributions from the rods and other attached objects. Key properties of **body objects** include:

- Mass and center of mass
- Volumetric displacement, assumed to be at the reference point
- Moment of inertia about each axis
- Hydrodynamic drag coefficients for each direction
- Added-mass coefficients for each direction

These parameters enable the simulations of even complex dynamics, such as rotations and translations within the mooring system, capturing both hydrodynamic and mechanical interactions. Points, rods, and bodies can all move freely or be coupled to an external program that

drives their motions. During runtime, the equations of motions of these objects are all integrated to advance each time step using different user-specified integrators, such as Runge-Kutta 2 or 4.

Using the open-source MoorDyn library, we implemented a dynamic cable simulation to model a vertical cable running from a platform to the seabed. For this simulation, we introduced multi-harmonic excitation by applying prescribed motions to the platform. Following (Matthew Hall et al., 2021), we implemented a subsea power cable model and selected the following cable parameters as an example to showcase the implementation of the B-NES devices. The cable had a diameter of 0.076 m and a mass density in air of 4.73 kg/m. The axial stiffness (EA) is set to 9 MN, and the bending stiffness (EI) of the cable is set to 11.71 kN-m^2. The added-mass coefficients, normal to the cable (Can), are equal to 1.0 and describe the influence of the surrounding water on the cable's inertia. The hydrodynamic drag coefficients, both normal (Cdn) and tangential (Cdt), are 1.2 and 0.008, respectively. This comprehensive setup allows us to simulate the dynamic behavior of the cable, including the effects of axial and bending stiffness, internal damping, seabed contact, and hydrodynamic drag, ensuring that the cable's response to multi-harmonic excitation is accurately modeled.

2.2. Analytical and numerical implementation

The analytical modeling of the B-NES integrated into a subsea dynamic power cable involves characterizing the dynamic responses of the B-NES to external excitations. A reduced-order model of the B-NES was created in the form of a nonlinear single-DOF system that consists of a mass that is connected to the subsea cable through two inclined spring-damper pairs with nominal stiffness k_i and damping coefficient d_i (see Fig. 2a). The inclined elements are set at an initial angle of inclination ϕ_0 relative to the point of attachment to the cable when the system is at rest, and it is assumed that these inclined elements are unstretched at equilibrium (Mojahed et al., 2018). Even though the spring and damper elements are linear, strong geometric nonlinearity is generated during the oscillation of the mass of the B-NES.

Referring to Fig. 2a, the mass M of the B-NES is connected by the inclined springs and dampers to the cable through a rod, which allows for adjustments of the initial angle of inclination ϕ_0, i.e., the angle of inclination at the equilibrium position of the B-NES. This connection directly affects the system's bi-stable nonlinear behavior. This angle significantly influences the response of the B-NES, as the natural length L of the inclined springs depends on this angle. In this configuration, the geometric nonlinearity enhances vibration mitigation by introducing bi-stability into the dynamics. Assuming that a disturbance (unwanted vibration) is applied to the cable, that the mass M of the B-NES executes vibrations in a direction that is orthogonal to the cable, and that its relative deflection (with respect to the local motion of the cable) is $x(t)$, the nonlinear vibration of the B-NES is governed by the following differential equation,

$$M\left(\ddot{x}+\ddot{x}_{cable}\right)+F_{si}(x)+F_{di}(x,\dot{x})=0 \tag{2.2.1}$$

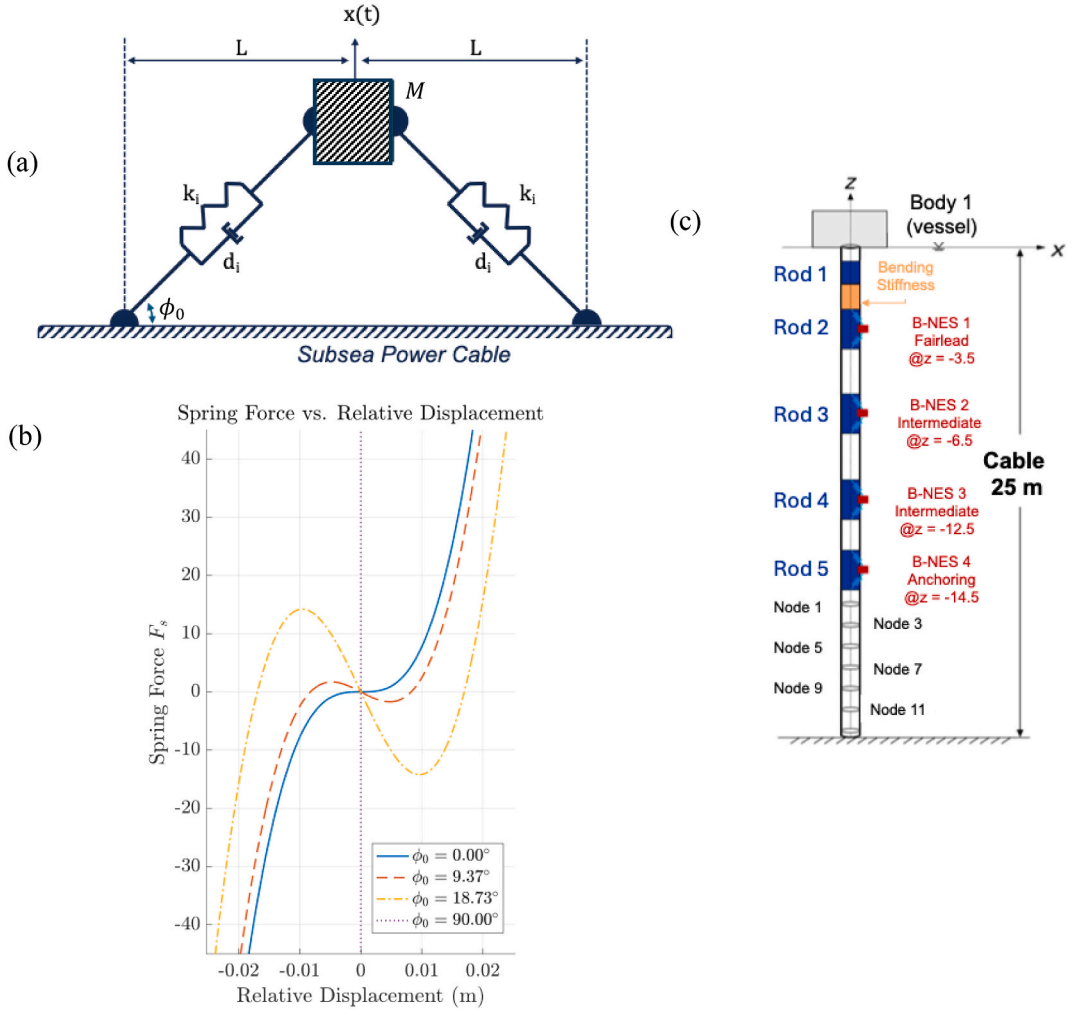

Fig. 2. (a) Schematic representation of the relative displacement of the B-NES mass with respect to the cable, where ϕ_0 is the initial angle of inclination at equilibrium, (b) tunability of the nonlinear stiffness of the B-NES with respect to ϕ_0, and (c) subsea power cable showing the locations of the four attached B-NESs.

where x_{cable} denotes the local motion of the cable at the points of attachment to the B-NES, $F_{si}(x)$ the stiffness force exerted by the inclined springs and $F_{di}(x,\dot{x})$ the dissipative force generated by the inclined viscous dampers. These are given by (Mojahed et al., 2018),

$$F_s = 2k_i\left(1-\frac{L\sec(\phi_0)}{\sqrt{L^2+y^2}}\right)y \tag{2.2.2}$$

$$F_{di} = 2d_i\frac{\dot{y}y^2}{L^2+y^2} \tag{2.2.3}$$

where $y = x + L\tan\phi_0$.

Depending on the angle of inclination at equilibrium ϕ_0, we can achieve different stiffness nonlinearities in the B-NES, as shown in Fig. 2b, where the nonlinear stiffness force F_{si} is plotted as a function of the relative displacement of the B-NES with respect to the cable to which it is attached; for these plots we considered the system parameters of (Mojahed et al., 2018), as follows, $M = 0.1\ Kg, k_i = 2\times10^4 N/m, d_i = 0.25 Ns/m, L = 0.05m,$ and different initial angles of inclination ϕ_0. Note that above a certain critical threshold of ϕ_0 we achieve *bi-stability*, i.e., two non-trivial stable equilibrium positions, with the trivial equilibrium in between being unstable (Mojahed et al., 2018). The oscillations of the mass between the two stable equilibria generate strong stiffness nonlinearity which, as shown below, is the source of the drastically enhanced vibration mitigation performance of the B-NES compared to the classical linear TMD.

In the following exposition, we incorporate the numerical model of the B-NES within MoorDyn and compare it to the previous analytical derivation in order to validate our modeling approach. Specifically, four B-NESs are attached to a vertical subsea cable, as shown in Fig. 2c. The cable was modeled as a lumped-mass system (see discussion in Section 2.1), and each B-NES was attached to it using a single rod element to maintain the desired angle of inclination, which is crucial for achieving bi-stability. The bi-stability is simulated numerically by adjusting the rod's length to alter the angle of inclination. Instead of the inclined linear springs, we modeled the elastic connections of the B-NES to the cable as linear elastic cords in-tension within MoorDyn, which introduces substantial nonlinearity through geometric and kinematic effects, as shown in Fig. 2b. The bi-stability is manipulated by varying the ratio of the natural lengths of the springs relative to the rod length: The smaller this ratio is, the greater the angle of inclination becomes, thus enhancing the bi-stable feature, as evidenced in the corresponding force-deflection stiffness characteristic of the B-NES (see Fig. 2b).

The unique aspect of this setup is the clearance effect introduced by the linear inclined elastic cords in-tension, which do not exert force unless the displacement of the B-NES mass relative to its attachment point exceeds their natural lengths. This feature introduces a significant nonlinearity that allows for the exploration of rich dynamics. The rod at the base of the B-NES is aligned along the cable, with the B-NES mass permitted to move in a perpendicular direction with respect to the cable segment to which it is attached. This setup paves the way for deriving analytical solutions to validate the numerical model's predictions. To ensure valid comparisons across different models, we adjusted the cable's mass density to uniformly distribute mass and negate any added-mass effects when comparing baseline scenarios with and without the addition of the B-NES devices. These comparisons have confirmed that the introduction of the rod element has minimal impact by ensuring consistent fairlead tensions across all tested configurations.

Fig. 3 demonstrates the analytical versus numerical results of the nonlinear force-deflection characteristics of the B-NES device for the system parameters in (Mojahed et al., 2018), and three different initial

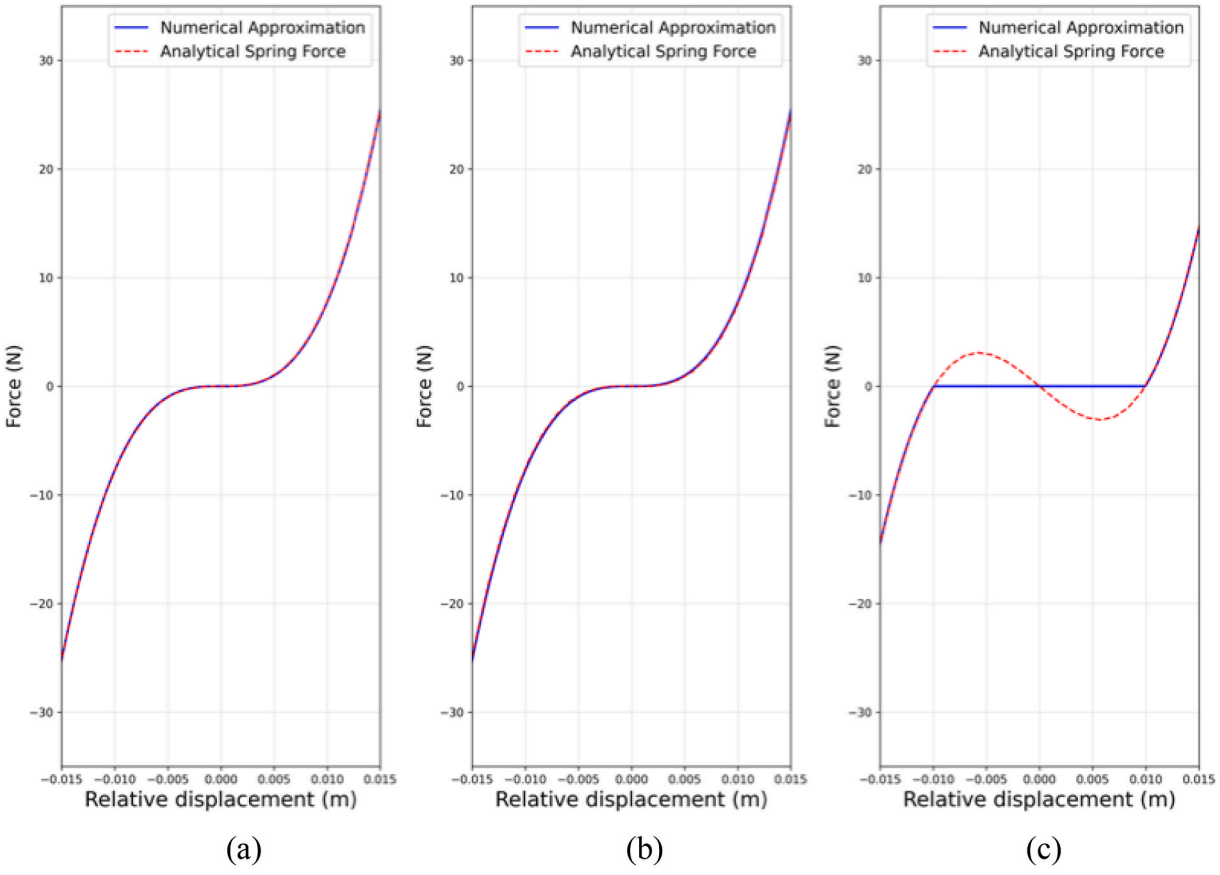

Fig. 3. Validation of the MoorDyn numerical simulation through comparison of force versus displacement curves for (a) $\phi_0 = 0°$ resulting in cubic stiffness, (b) $\phi_0 = 2°$, and (c) $\phi_0 = 11.48°$.

angles of inclination ϕ_0. More specifically, in Fig. 3a, we consider the nonlinear stiffness of the B-NES with zero angle of inclination, where we have a realization of pure cubic stiffness nonlinearity due to the relative transverse motion of the B-NES mass in the orthogonal direction with respect to the subsea cable segment to which it is attached. In Fig. 3b and c, we increase the initial angle of inclination by adjusting the length of the attaching rod to a resulting angle of inclination equal to $\phi_0 = 2^\circ$ and $\phi_0 = 11.48^\circ$, respectively. As expected, the results differ in the regime where the inclined cords are slack. Because they do not exert any force on the cable, the bi-stable behavior yields a sudden transition ("jump") between the two non-trivial stable equilibrium positions. This result also shows the difference between our numerical modeling, which is based on the inclined cords-in-tension within MoorDyn, and the analytical model (2.2.3), which is based on linear springs. We note, however, that the "jumps" that we achieve in the MoorDyn model add extra-strong nonlinearity in the dynamics of the B-NES and emphasizes even more its bi-stability behavior; as such, the resulting non-smooth effects in the dynamics of the B-NES play an even more beneficial role for vibration mitigation.

3. Optimization of the B-NES

An advanced data-driven methodology is developed to optimize the operational performance of the NES for dynamic stabilization of the subsea power cable. This discourse elucidates an exhaustive optimization strategy, from computational configurations to the rigorous assessment of performance indices, all underpinned by advanced High Performance Computing (HPC) resources.

At the core of our computational strategy is the utilization of the Hardware-Accelerated Learning (or HAL) cluster, an HPC cluster at the University of Illinois Urbana-Champaign, which is thoroughly engineered to facilitate the demanding computational tasks that are inherent to the present research task. Contrary to conventional parallel computations performed on standard desktop configurations, our approach leverages 96 CPUs, thereby substantially diminishing the computational latency for scenarios characterized by high mechanical stiffness of the B-NES. This computational efficiency is decisive given the extensive parameter space and the large volume of simulations—exceeding 10,000 discrete evaluations—necessary to thoroughly canvass and optimize the potential configurations of the B-NES. For efficient management and distribution of the simulation tasks across the HPC infrastructure, we employ the SLURM job scheduling system. This system not only optimizes the allocation of computational resources but also guarantees that each simulation is executed under stringent and reproducible conditions, crucial for the empirical validity of our results.

The optimization methodology adopted in this work encompasses a detailed parametric study, systematically varying critical properties of the B-NES—such as stiffness, damping characteristics, and mass—to detect configurations that deliver optimal vibration suppression efficacy. This process is facilitated by the application of HPC simulations integrated with a Python toolkit based on the code MoorPy (M. Hall et al., 2021), designed to streamline file operations and preprocessing for MoorDyn simulations. In our optimization framework, we explore both isolated and multiple B-NES configurations attached at different positions along the subsea cable, particularly focusing on zones of the cable identified as high risk for structural failure. We strategically position multiple B-NES devices near the fairlead—where the cable connects to the platform, a juncture deemed critical for cable integrity (Strang-Moran, 2020). In our simulations, we consider multi-harmonic pulse (transient) excitations imposed by platform motion, thereby enabling early interception of vibrational energy by the B-NES positioned near the excitation source, with the aim of mitigating cable vibration amplitudes before the vibration disturbance can propagate further down along the cable. Further, we deploy additional B-NESs at antinodes of cable modes where oscillation amplitudes are expected to peak, thereby impacting not only the local but also the global dynamics of the cable, as observed in extensive simulation trials. To optimize the performance of the B-NESs, we adjust the axial stiffness parameters corresponding to the stiffnesses of the cords-in-tension of various B-NES configurations implemented along the cable's length. Accompanying these adjustments, proportional damping in the cords-in-tension is modulated in accordance with stiffness variations to maintain model fidelity. Throughout these simulations, the additional mass effect to the cable (due to augmentation of the cable by the B-NESs) is rigorously accounted for by equating the total masses of the baseline cable configuration (i.e., the cable with no B-NES attached) and the cable with NESs attached.

A comprehensive suite of simulations facilitates the implementation of B-NES design, optimizing device performance across varying excitation frequencies and amplitudes. Concurrently, we define three quantitative performance metrics to rigorously evaluate device efficacy:

(i) The Δ (Delta) measure, reflecting kinetic energy changes in the subsea cable induced by the B-NESs;
(ii) The Γ (Gamma) measure, assessing the corresponding potential energy changes in the cable; and
(iii) The settling time t*, quantifying the rate at which the B-NESs dissipate the vibrational energy of the subsea cable.

These metrics, which are presented in detail below and are derived from detailed mathematical formulations and empirical observations, enable the precise assessment of the performance of the B-NESs on cable dynamics subject to varying operational conditions. This optimization approach, supplemented by logarithmic scaling of parameter variations (to account for large disparities in the B-NES parameter values), provides a robust framework for identifying optimal B-NES configurations through a systematic and exhaustive exploration of performance landscapes, culminating in a Pareto-optimal selection strategy that aligns the B-NES system parameters to specific operational requisites.

The first metric, Δ, monitors the reduction in the kinetic energy of the cable due to the action of the attached B-NESs. This metric is defined as follows,

$$\Delta = \frac{\sum_{i=1}^{N} \frac{1}{2} \int_{t_0}^{t_1} m_i \left(\frac{dx_{CN}^i(t)}{dt}\right)^2 dt}{\sum_{i=1}^{N} \frac{1}{2} \int_{t_0}^{t_1} m_i \left(\frac{dx_C^i(t)}{dt}\right)^2 dt} \tag{3.1}$$

where m_i is the mass of the i-th (discretized) segment of the cable, and $x_C^i(t)$ and $x_{CN}^i(t)$ denote the corresponding deflections of the node of the cable without and with NESs attached, respectively. The time integrations in the numerator and denominator are carried out for the time window of the response $t \in [t_0, t_1]$. It follows that this positive measure can be used to assess how the action of the B-NESs affects the kinetic energy of the cable. Clearly, the smaller Δ is, the more effective the B-NESs become in reducing the kinetic energy of the cable. Similarly, the second performance metric Γ measures the reduction in the potential energy of the cable when the B-NES are added and is defined as:

$$\Gamma = 1 - \frac{\sum_{i=1}^{N} \frac{1}{2} \int_{t_0}^{t_1} {x_{CN}^i}^2 dt}{\sum_{i=1}^{N} \frac{1}{2} \int_{t_0}^{t_1} {x_C^i}^2 dt} \tag{3.2}$$

Lastly, the settling time t^* is a measure that quantifies how fast the B-NESs manage to dissipate the vibrational energy of the subsea cable. Referring to Fig. 4, this measure is defined as the time $t = t^*$ when the measure,

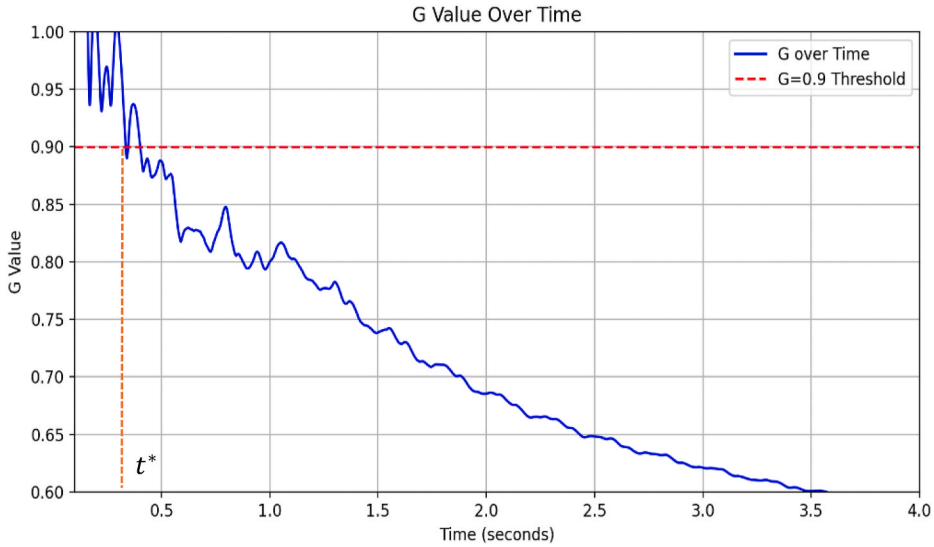

Fig. 4. Defining the settling time t^* from G(t).

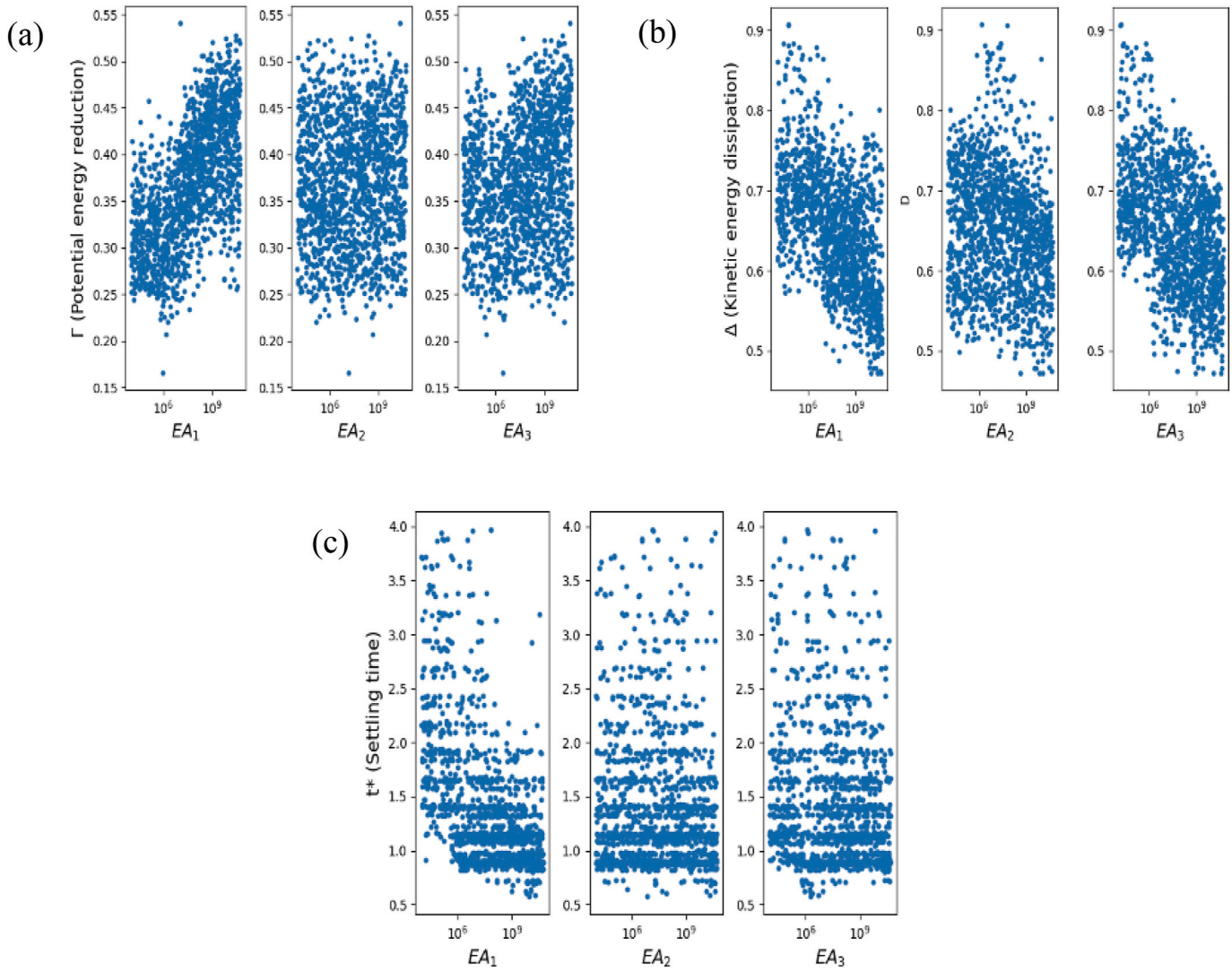

Fig. 5. Optimization of the axial stiffnesses of the cords-in-tension of the three B-NES types: (a) measure Γ, (b) measure Δ, and (c) settling time t^*.

$$G(t) = 1 - \frac{\sum_{i=1}^{N} \frac{1}{2} \int_0^t x_{CN}^{i\,2} dt}{\sum_{i=1}^{N} \frac{1}{2} \int_0^t x_C^{i\,2} dt} \tag{3.3}$$

decreases for the first time to the value $G(t^*) = 0.9$, i.e., when the integral of the potential energy of the cable with B-NESs reaches 10 % of the corresponding integral for the cable with no attached B-NESs for the first time.

In the optimization, we utilize logarithmic scaling for the parameter variation, which is more effective than linear scaling when exploring parameter ranges that are orders of magnitude apart. In the optimization procedure, four B-NESs were strategically placed along the length of the subsea cable to provide vibration mitigation at critical points; these devices are categorized into three types: Fairlead, Intermediate-Antinode, and Anchoring (see Fig. 2c). The Fairlead B-NES 1, positioned closest to the platform, is followed by the Intermediate-Antinode B-NESs 2 and 3, with the Anchoring B-NES 4 located at the end of the cable. This arrangement ensures that the B-NESs are positioned at vital locations along the cable, offering enhanced protection to key points. The prescribed multi-harmonic transient motion of the platform is given by,

$$F(t) = A\ sin\ \omega t + A\ sin\ 2\ \omega t + A\ sin\ 4\ \omega t, t \leq 0.5\ \text{s} \tag{3.4}$$

$$F(t) = 0, t > 0.5\ \text{s}$$

with $\omega = 2\pi f, f = 2$ Hz, $A = 0.01$ m. A total of 2000 simulations were performed to optimize the three types of B-NESs attached to the subsea cable. The optimization considered the variations in the axial stiffnesses $EA_i, i = 1, 2, 3$, of the inclined cords-in-tension of the three B-NES types (because these are key parameters) in the range $EA_i \in [10^4\text{N}, 5 \times 10^{10}N]$. The remaining B-NES parameters (angle of inclination, natural lengths of the cords, and mass) were kept fixed, as listed in Table 1.

We note that the selected angle of inclination of $\phi_0 = 3.562^0$ is greater than the bifurcation value for bi-stability, which in this case is $\phi_{0,bif} = 0.22^0$ as predicted by the analytical formula derived in (Mojahed et al., 2018); this guarantees that all four B-NESs possess the bi-stability feature (this is also verified by the numerical transient responses that follow). Moreover, we note that the mass of B-NES 1 was taken as 4.5 % of the total cable mass, the masses of B-NES 2 and 3 as 3.5 % and 4.5 % of the cable mass respectively, and the mass of B-NES 4 as 4.5 % of the cable mass (see Fig. 2c). Proportional damping was considered in the cords-in-tension, so the coefficients of the inclined viscous dampers were taken always proportional to the respective axial stiffnesses of the cords in the range [4.472 Pa − s, 9, 999.7 Pa − s]. In Fig. 5 we depict the variations in the three performance measures in terms of the variations in the three axial stiffnesses for all 2000 realizations (simulation runs). The aim of the optimization of the dynamics of the cable was to (i) maximize the potential energy reduction measure Γ, (ii) minimize the kinetic energy measure Δ, and (iii) minimize the settling time t^*. By doing so, we sought the optimal combination of the three B-NES types that mitigates the vibrations of the cable in the least possible time.

In Fig. 6, we systematically identify an optimal configuration, manifesting as a Pareto front, through a multi-dimensional representation of performance metrics across various parameter planes, This Pareto front features the most optimal parameter sets, tailored to specific operational requirements. In the scenario examined, we extract the parameters of the B-NESs as shown in the first two columns of Table 1, corresponding to optimized performance with respect to the metrics (with optimal values),

$$\Delta = 0.5064, \Gamma = 0.5201 \text{ and } t^* = 0.896$$

By employing the proposed optimization framework, we evaluate the efficacy of the B-NES devices across various simulation environments, facilitating the generation of a comprehensive 3D parameter space representation, as shown in Fig. 6c. This spatial visualization aids in the strategic selection of the B-NES configurations by integrating all performance metrics into a single plot. Subsequently, we refine our selection process to isolate the optimal solution, ensuring it aligns with the complex dynamics of subsea cable systems. This approach not only enhances our understanding of the B-NESs' operational effectiveness but also provides a robust framework for deploying these devices in real-world scenarios, optimizing their performance to meet the stringent demands of dynamic subsea environments.

The optimal configuration of the B-NESs (Table 1) was rigorously tested to highlight and understand the dynamic interactions that govern the optimal vibration suppression of the tested subsea power cable. In Figs. 7 and 8, we depict the significant reduction in the cable vibrations enabled by the B-NESs given the excitation profile (3.4). For comparison, we show also the corresponding responses of the "unprotected" cable (Section 2.1), which incorporate the masses of the four B-NESs so that no mass-added effects distort the results. There is global mitigation of vibrations in the cable. The nonlinear beneficial effects of the B-NESs are not restricted to their points of attachment but extend to the entire cable.

The beneficial vibration suppression of the subsea cable vibrations by the B-NESs relies on two effects: (i) nonlinear targeted energy transfer (absorption) of broadband energy from the cable to the B-NES, where this energy is localized and dissipated, and (ii) rapid nonlinear "scattering" of vibration energy of the cable to higher frequencies within the cable itself. Indeed, such low-to-high energy transfer within the subsea cable yields an immediate attenuation of the cable vibrations (because the oscillation amplitudes decrease with increasing frequency); moreover, higher-frequency vibrations can be more effectively dissipated by the inherent dissipative capacity of the cable itself, compared to lower-frequency ones. We note that the bi-stability feature of the NESs significantly enhances vibration energy scattering from low to high frequencies within the subsea cable.

We now demonstrate the nonlinear energy scattering in the cable dynamics in the frequency domain, that is induced by the B-NESs. This is achieved by postprocessing the transient responses of Fig. 7 using numerical wavelet transform (WT) analysis. The WT is a powerful tool for time-frequency analysis and is particularly advantageous when dealing with transient, non-stationary signals such as those in our study. Unlike the conventional Fourier transform, which assumes that the signal is stationary and provides an averaged frequency representation, the WT is applicable to non-stationary signals (such as the nonlinear transient responses considered herein). As such, the WT enables localized frequency analysis, offering temporal resolution that captures the evolution of the main frequency components of the signal over time. This adaptability is crucial for dynamic analysis that seeks to track the transient evolutions of the frequency components of a measured signal.

Table 1
Optimal parameters for the three types of B-NESs (see Fig. 5).

B-NES type	EA_i (N)	d_i (Pa-s)	φ_0 (deg)	Natural length of cord-in-tension (m)	Mass (kg)
1. Fairlead	5.384×10^8	1.038×10^3	3.562	0.5	4
2. Intermediate-Antinode	7.293×10^9	3.819×10^4	3.562	0.5	3
3. Intermediate-Antinode	1.067×10^9	1.460×10^3	3.562	0.5	4
4. Anchoring	1.067×10^9	1.460×10^3	3.562	0.5	4

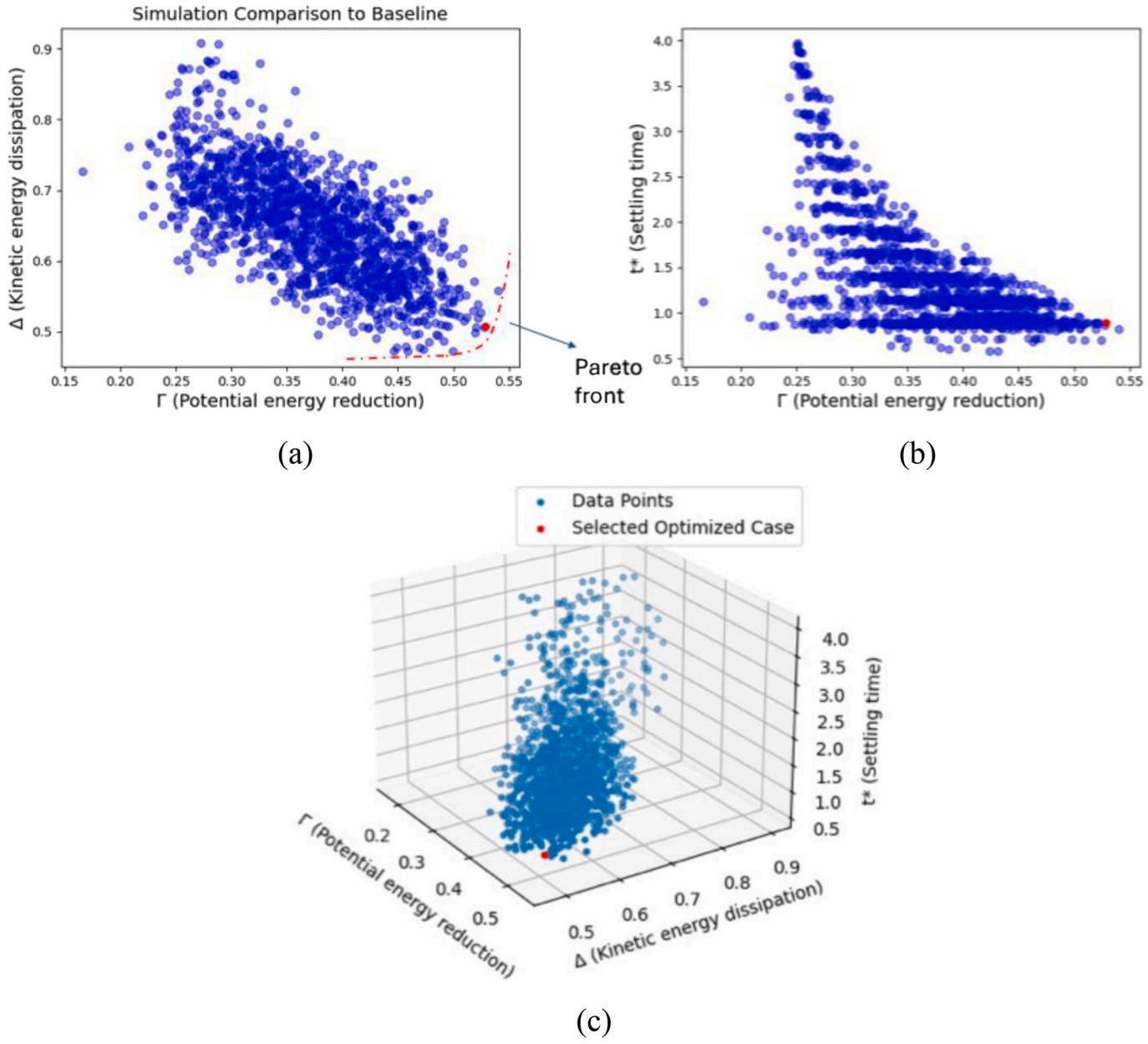

Fig. 6. Multi-dimensional representation of the performance metrics for the 2000 simulation runs (data points) of the optimization; the optimal case is denoted by the red dot. (For interpretation of the references to colour in this figure legend, the reader is referred to the Web version of this article.)

To apply a numerical continuous WT, we selected the Morlet wavelet (Addison, 2017), a complex wavelet family $\psi(t)$ known for effectively separating the phase and amplitude of harmonic components within a signal. This wavelet family is defined as,

$$\psi(t) = \pi^{-\frac{1}{4}} \left(e^{i\omega_c t} - e^{-\frac{\omega_c^2}{2}} \right) e^{-\frac{t^2}{2}} \tag{3.5}$$

where ω_c represents the central frequency of the wavelet, allowing us to focus on specific frequency bands within the signal. Then, given a signal x(t), its continuous WT is expressed as,

$$X(\omega, t) = \frac{\omega}{\sqrt{\pi}\omega_c} \int_{-\infty}^{\infty} x(s) \left(e^{-i\omega(s-t)} - e^{-\frac{\omega_c^2}{2}} \right) e^{-\frac{(s-t)^2}{\alpha^2}} ds \tag{3.6}$$

where $X(\omega, t)$ is the complex WT of x(t). Given that this is a two-dimensional complex function of frequency and time, we typically study contour plots of its magnitude, $|X(\omega, t)|$.

In Fig. 9 we depict the contour plots of the modulus $|X(\omega, t)|$ of the WT of the transient nonlinear responses of Fig. 7. These results reveal the mitigation effect of the B-NESs on the cable vibrations and explain the governing nonlinear dynamics that cause it. We note the much shorter duration of *both* dominant lower-frequency harmonics of the cable dynamics (introduced by the multi-frequency excitation) when the optimized B-NESs are attached (Fig. 9b) compared to the unprotected cable (Fig. 9a)—*this demonstrates the efficacy of the B-NESs to mitigate multi-harmonic vibrations of the cable*.

As discussed previously, this vibration mitigation effect is caused (i) by targeted energy transfer (unidirectional absorption) of multi-frequency vibration energy from the cable to the B-NESs, where the transferred energy is locally confined and rapidly dissipated, and (ii) by nonlinear scattering of the vibration energy of the cable from low to high

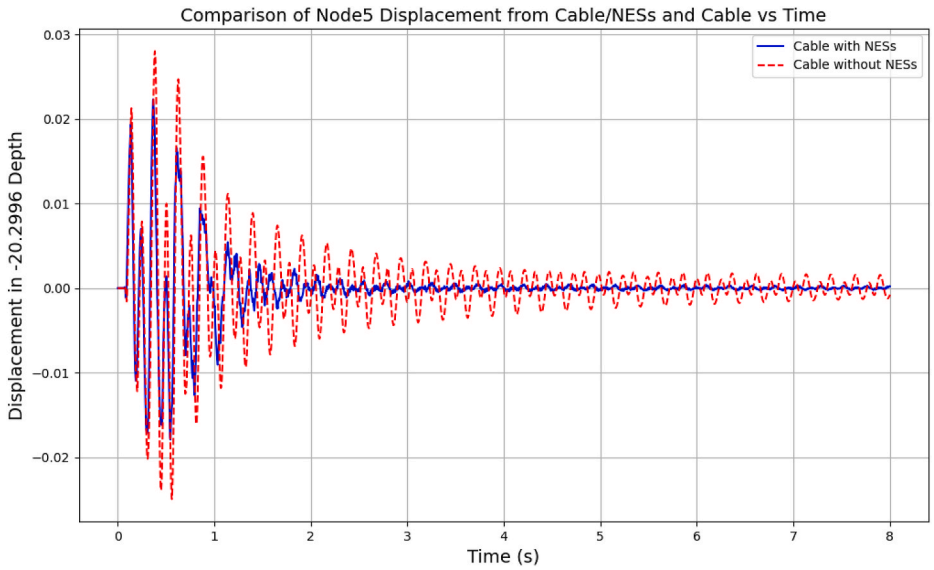

Fig. 7. Transient displacement (in m) at node 5 (at a depth 20.2996 m; see Fig. 2c) of the subsea cable for the cases with and without optimized B-NESs attached; note the high-frequency and low-amplitude vibrations as time increases, caused by nonlinear scattering of cable vibrations at high frequencies by the B-NESs.

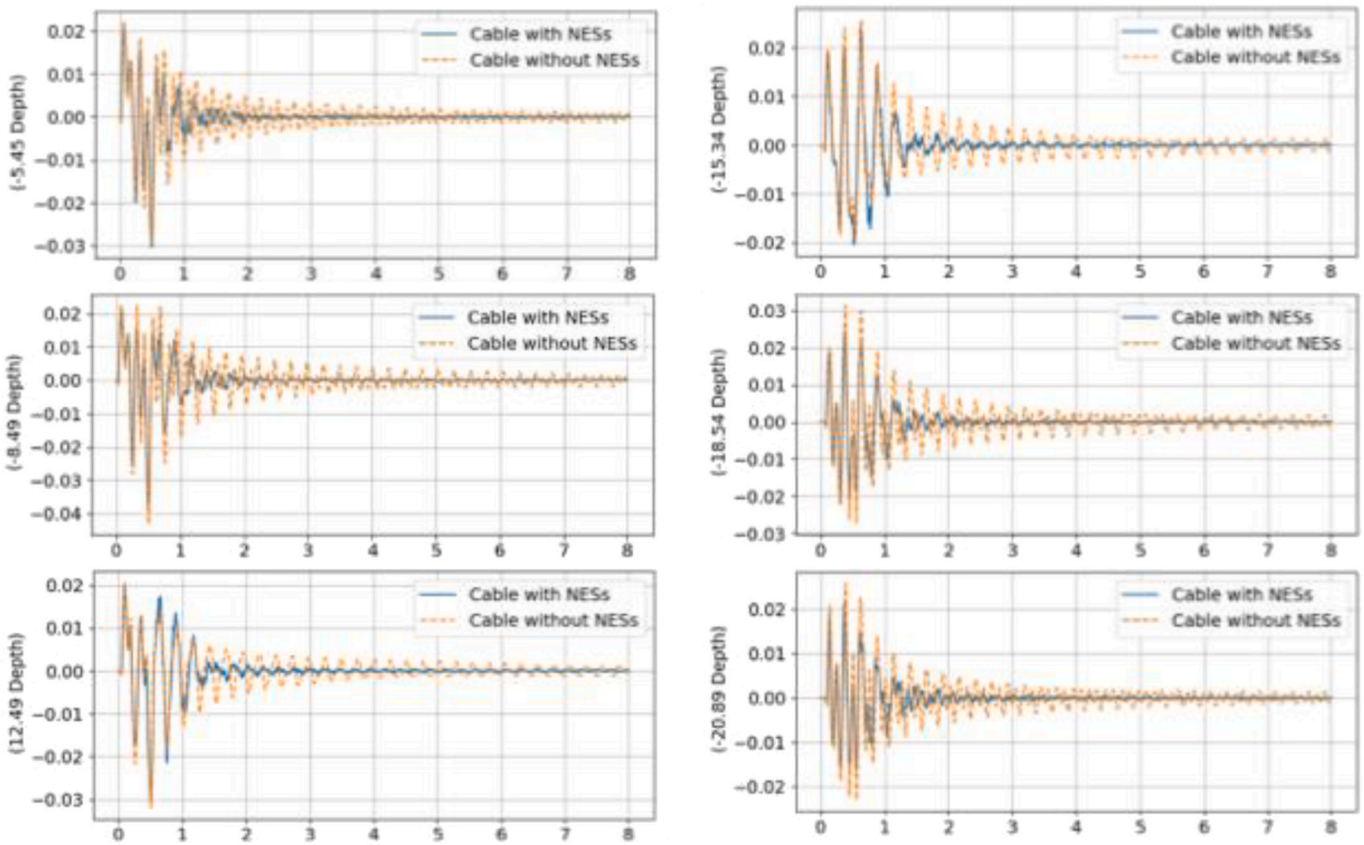

Fig. 8. Transient displacements (in m) at different locations along the subsea cable, with optimized attached B-NESs and with no B-NESs attached to showcase the global effects of the B-NESs over the entire length of the cable dynamics.

frequencies (Fig. 9b). This effect is followed by a marked suppression of all lower harmonics of the cable dynamics and underscores the B-NESs' capacity to passively adapt their resonances to multi-frequency excitations and, by doing so, to achieve *broadband vibration suppression of the cable*. Clearly, no such effects can be achieved by any linear design, e.g., the classical TMD, due to the narrowband operation of such devices and their inability to address multi-harmonic transient vibrations of the cable at broad frequency ranges.

To gain deeper insight into the nonlinear vibration mitigation of the cable due to the action of the optimized B-NESs, we examined the relative transient response of each B-NES with respect to the motion of the cable at its corresponding point of attachment (Fig. 10). As a further step, we employed a WT to postprocess the relative responses of Fig. 10, providing insight into the transient evolution of the dominant harmonics

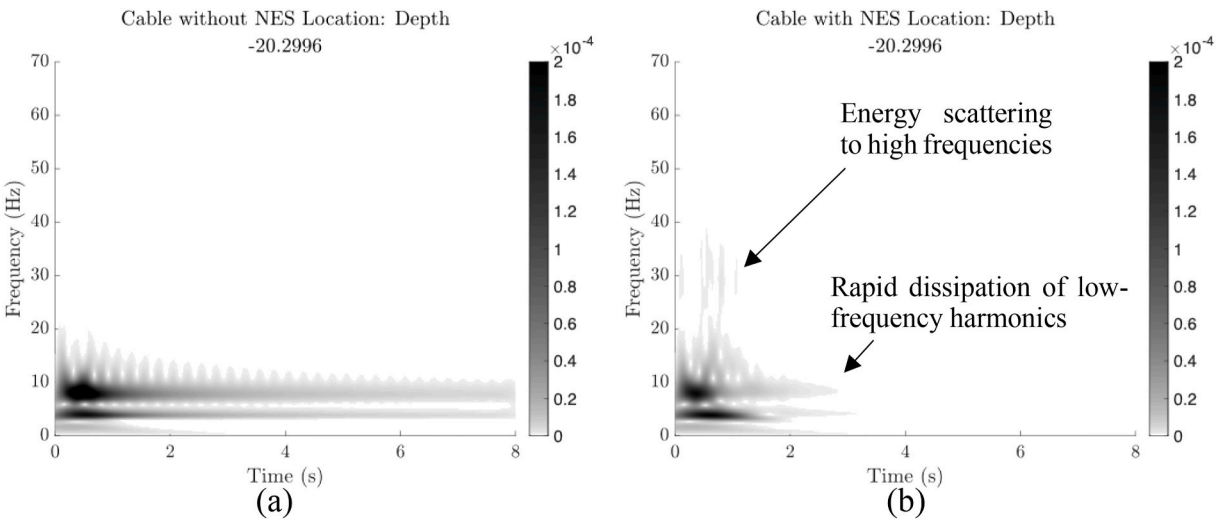

Fig. 9. Contour plots of the magnitude $|X(\omega, t)|$ of the WT of the cable responses of Fig. 7 for the case (a) without and (b) with (optimized) B-NESs, where more heavily (lightly) shaded regions in the contour plots correspond to stronger (weaker) harmonics. Note the low-to-high-frequency vibration energy scattering in (b) due to the action of the B-NESs.

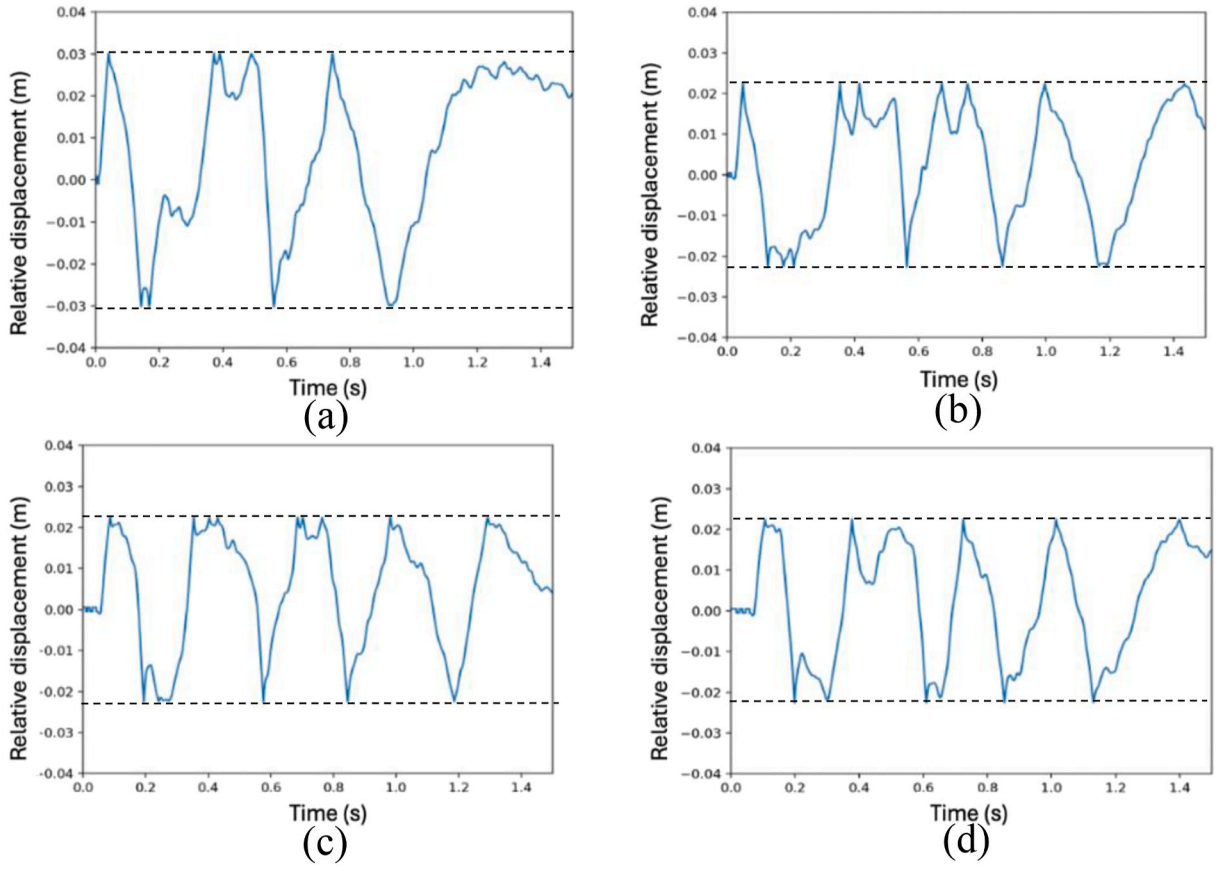

Fig. 10. Relative displacement of each optimized B-NES with respect to their point of attachment to the cable: (a) Fairlead, (b,c) Intermediate-Antinode, (d) Anchoring (see Fig. 2c). Dashed lines indicate the points of "jumps" signifying bi-stability, i.e., sudden cross-well transitions of the dynamics between different stable equilibria.

of the relative response of the B-NES. In this way, we can study how each B-NES absorbs broadband energy from the cable through resonance capture (Vakakis et al., 2009) and how each B-NES operates as a "nonlinear scatterer" of vibration energy from low to high frequencies. As discussed previously, this latter feature promotes a highly effective mechanism for rapid vibration mitigation. The WT results are shown in Fig. 11.

As anticipated, the B-NESs exhibit cross-well oscillations, a phenomenon rooted in the bi-stability characteristics intrinsic to their design. This bi-stable behavior is critical to the B-NESs' ability to effectively scatter the vibrational energy of the cable. A detailed study of the relative displacements between each optimized B-NES mass and its

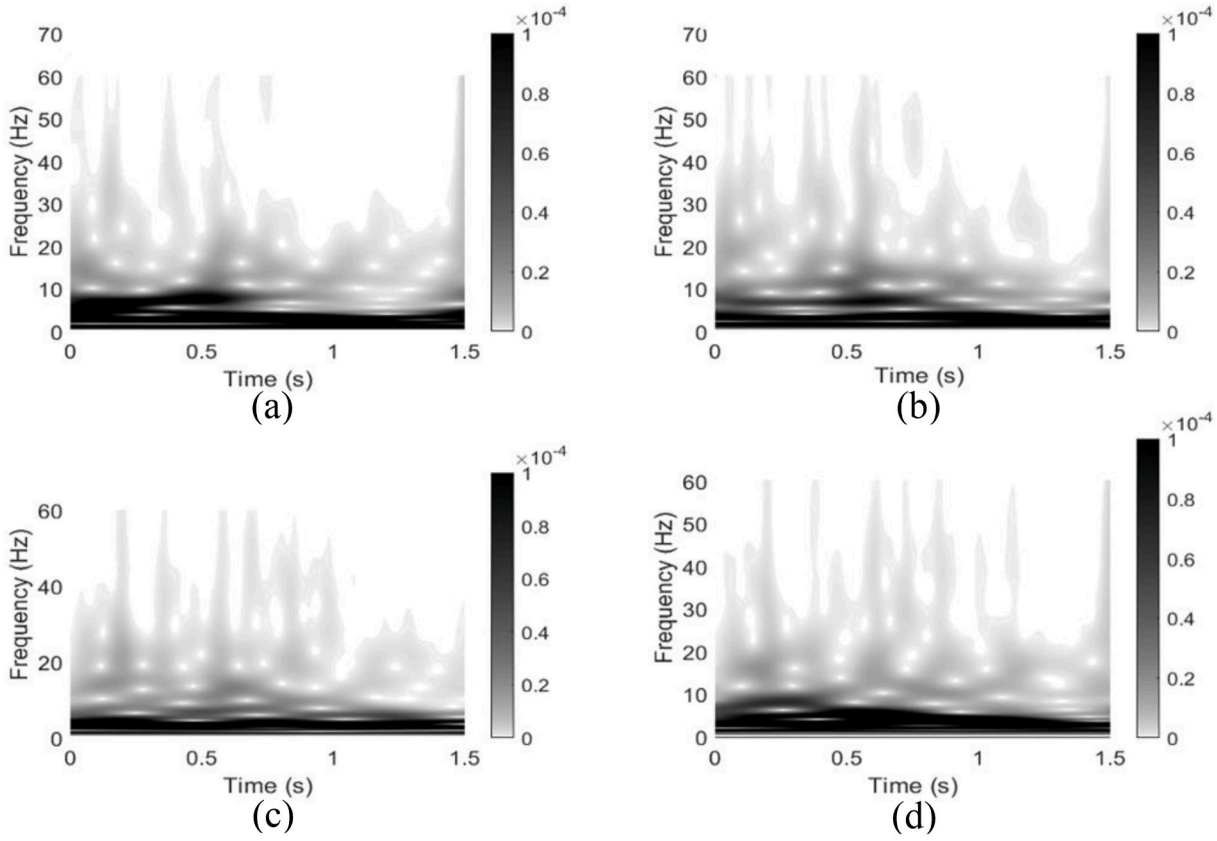

Fig. 11. Contour plots of the magnitudes of the WT of the relative displacements of the optimized B-NESs in Fig. 10. Note the intense nonlinear low-to-high-frequency energy scattering.

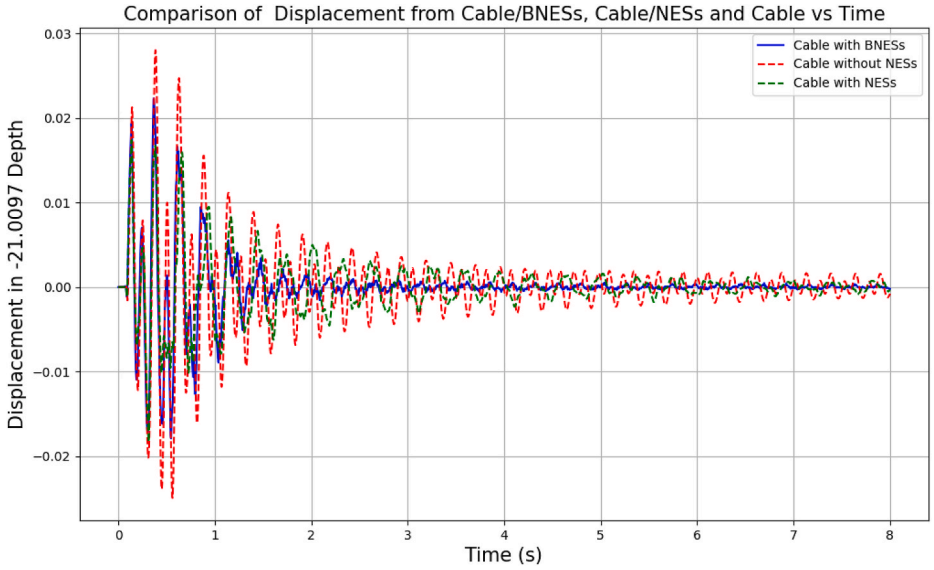

Fig. 12. Transient displacement (in m) at node 5 (at a depth 20.2996 m – see Fig. 2c) of the subsea cable for the cases with B-NESs, with "plain" cubic stiffness NESs and with no NESs attached.

cable attachment point provides deeper insight into the B-NESs' operational dynamics. Indeed, each optimized B-NES demonstrates rapid response times and operates in a broadband fashion, i.e., both at lower and higher frequencies, showcasing their inherent passive tunability.

Passive tunability with respect to energy (and initial angle of inclination—see Fig. 2a) is a hallmark of the B-NES's nonlinearity, and this strongly nonlinear device is intentionally designed with a complete absence of a preferential resonance frequency; rather, its instantaneous resonance frequency solely depends on its instantaneous energy, so it can passively adapt (tune) its resonance to excitations of varying intensity (Vakakis et al., 2009). The resulting tunability of the B-NES resonance frequency makes it exceptionally suited for handling broadband and highly non-stationary excitations (cable vibrations) of the type that are typically encountered in VIV scenarios. This capability

underscores the B-NES's robust mitigation efficacy and its capacity to dynamically adapt to and mitigate complex vibrational patterns across changing operational conditions.

The effect of bi-stability on the cable mitigation is further highlighted when comparing the performance of the previous B-NESs with "plain" NESs without bi-stability features. These NESs are obtained by setting the initial angle of inclination (i.e., angle at equilibrium) to $\phi_0 = 0^0$ (see Fig. 2b) and reducing the axial stiffnesses of the cords-in-tension. Then we obtain a purely cubic nonlinear stiffness characteristic for each NES as shown in Fig. 3a (Mojahed et al., 2018) and complete elimination of the bi-stability phenomenon. This is an extra manifestation of the tunability of the NESs with respect to geometry. This can be implemented in MoorDyn simply by adjusting the ratio of the natural lengths of the cords relative to the rod length to a value of 1. Table 2 provides the specific parameters for the set of four plain NESs.

Under the same multi-harmonic excitation conditions described previously, Fig. 12 presents a comparison of the mitigating performance of the B-NESs and the plan NESs, which clearly demonstrates that while the cable equipped with plain NESs exhibits reduced oscillation amplitudes, the optimized B-NESs are notably more effective in mitigating the cable vibrations. This enhanced performance is attributed to the bi-stability effect, which provides the extra capacity of the B-NESs to rapidly scatter vibration energy from low-to-high frequencies, and by doing so, more efficiently dissipating the vibration energy.

In synopsis, a critical aspect of the B-NES's functionality is its capacity to tune its resonance frequency as the energy and frequency content of the transient vibration varies. Unlike linear systems that are constrained by fixed resonance frequencies, the B-NES showcases a unique adaptability where its response (resonance) frequency diminishes concomitantly with energy levels. This characteristic not only enhances the passive tunability of the B-NES across a broader frequency spectrum but also drastically improves its mitigation effectiveness in diverse operational scenarios by dynamically adjusting to the energy and frequency profile of the induced vibrations. This energy-dependent frequency adjustment exemplifies the B-NES's superior adaptability compared to traditional linear vibration mitigation devices, providing a tailored response to the specific energy conditions encountered in subsea environments. On top of that, the extra bi-stability feature enables rapid uni-directional (targeted) energy transfer from low-to-high frequencies, which, in turn, quickly reduces the vibration amplitude and dissipates the vibration energy more effectively.

4. Robustness analysis of the B-NES

In this section, we investigate the robustness of the B-NES in mitigating vibrations of dynamic subsea cables by incorporating stochastic excitations that model real-world uncertainties. We also account for variations in the cables' dynamic properties due to environmental factors such as biofouling, demonstrating the B-NES's ability to adapt and maintain effective vibration control under changing operational conditions.

To demonstrate the robustness of the B-NES under the varying environmental conditions in which the subsea power cable operates, we incorporate stochasticity into the excitation force by employing a custom excitation function. This function includes random variations in amplitude, frequency, and phase, thereby emulating realistic stochastic conditions. Specifically, the excitation at each time step i of the active time duration of the excitation is defined as,

$$F(i) = \sum_{j=1}^{3} A_{variation}[j] \cdot \sin(i \cdot \omega_{variation}[j] + \phi[j]) + Noise(i),$$

where $A_{variation}[j] \sim \mathcal{N}(A, 0.1 \cdot A)$ introduces random variations in amplitude, $\omega_{variation}[j] \sim \mathcal{N}(\omega_{base}, 0.05 \cdot \omega_{base})$ introduces frequency shifts, $\phi[j] \sim \text{Uniform}(0, 2\pi)$ applies random phase offsets and $Noise(i) \sim \mathcal{N}(0, noise\_level)$ adds small-scale Gaussian noise to the excitation. By saving the excitation parameters, including $A_{variation}$, $\omega_{variation}$, ϕ and Noise we ensured reproducibility and enabled detailed analysis. This stochastic approach effectively represents real-world subsea environments, where external forces are inherently unpredictable due to varying environmental disturbances. Furthermore, it provides a robust testing framework for evaluating the broadband capability and adaptability of the B-NES under dynamic and uncertain loading conditions.

In addition to uncertainties introduced by external forces, biofouling can alter the fundamental frequency of subsea cables by affecting their effective stiffness and mass distribution. To demonstrate the robustness of the B-NES, we simulated the effect of biofouling by varying the cable's diameter (D) and mass-in-air density (MassInairDens) in the ranges D = [0.08,\ 0.1,\ 0.12] m and MassInairDens = [5.73, \ 6.5,\ 7.5] kg/m.

In Fig. 13 we depict the FFT plots of the transient displacement of the subsea cable at node 5 (at a depth 20.2996 m; see Fig. 2c) for different combinations of cable diameter and cable mass density. Regarding the B-NES, leveraging the optimized solution described in Section 3, we applied the aforementioned stochastic excitation force—representing platform motion—to assess the robustness of the B-NES across all tested parameter variations. These FFT plots simulate the variability of the frequency content of the cable dynamics for biofouling and highlight the resulting shifts in resonance frequencies of the cable. This variability in the cable resonances necessitates the use of a broadband vibration mitigation device such as the B-NES of our work, which, being a strongly nonlinear devices, passively tunes (i.e., self-adapts) its resonance response to maintain its mitigation effectiveness over broad frequency ranges. Clearly, this is not possible using the conventional linear tuned mass damper (TMD), which has a fixed resonance frequency and so has drastically deteriorating mitigation performance off resonance.

Under nominal operating conditions (without biofouling), the B-NES achieved a 53.60 % reduction in RMS displacement following the excitation, serving as a baseline for its performance. In the scenarios representing biofouling effects shown in Fig. 13, the B-NES maintained its effectiveness, achieving reductions in RMS displacement ranging from 21.77 % to 50.37 % (see Fig. 14). These results highlight the device's ability to adapt to dynamic changes in cable properties caused by biofouling, without requiring any parameter adjustments. The transient displacement time-series shown in Fig. 14 confirm the robust mitigation performance of the B-NES in suppressing the vibrations of the dynamic cables. Indeed, the nonlinear features of the B-NES enable it to maintain control over broadband vibration, ensuring robustness under altered cable dynamics. This self-adaptability renders the B-NES a suitable and practical solution for real-world subsea cable applications, where environmental conditions like biofouling introduce uncertain and continuously varying operating scenarios.

Table 2
Parameters for the three types of plain NESs used for Fig. 12.

NES Type	EA_i (N)	d_i (Pa-s)	φ_0 (deg)	Natural length of cord-in-tension (m)	Mass (kg)
1. Fairlead	5.384×10^6	1.038×10^3	0	0.5	4
2. Intermediate-Antinode	7.293×10^6	3.819×10^3	0	0.5	3
3. Intermediate-Antinode	1.067×10^6	1.460×10^3	0	0.5	4
4. Anchoring	1.067×10^6	1.460×10^3	0	0.5	4

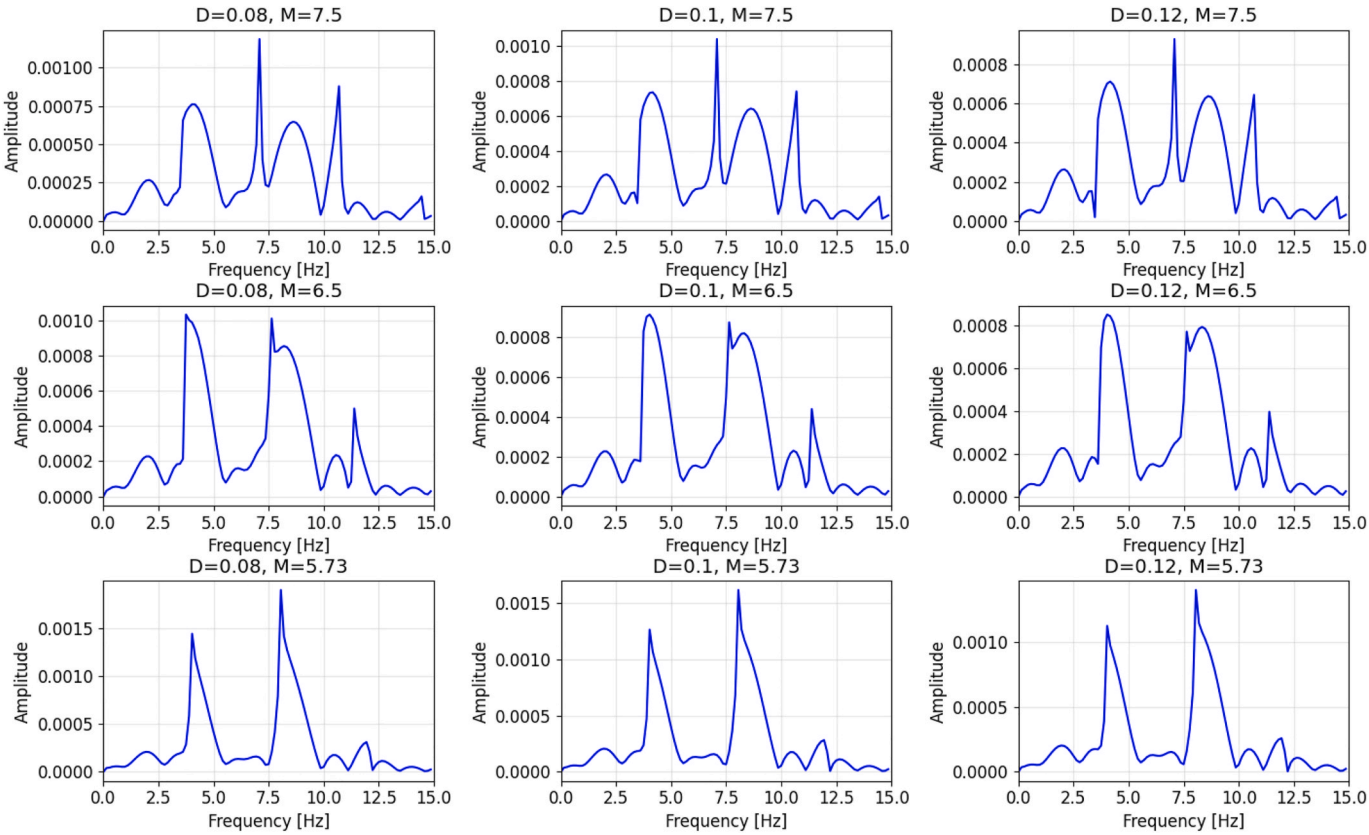

Fig. 13. FFT plots of the transient displacement at node 5 (at a depth 20.2996 m; see Fig. 2c) of the subsea cable showing the variability of the frequency content of the dynamical response of the cable for different combinations of cable diameter (D) and cable mass density (M).

5. Concluding remarks

In this work, we investigated the stabilization of dynamic subsea power cables typically used in offshore wind farms by means of B-NESs. These are strongly nonlinear passive absorbers with a capacity for mitigating broadband vibrations. The B-NES configuration is relatively simple, as it relies on an oscillating mass that is connected to the subsea cable by means of inclined spring-damper pairs. It is interesting that although these devices are composed of *linear* stiffness and dissipation elements, their dynamics is *strongly nonlinear* due to geometric and kinematic nonlinearities; that is, the nonlinearities are generated by the relative oscillation of the mass of a B-NES with respect to the point of attachment to the cable. We used a lumped-mass model to simulate the subsea cable's dynamics with or without B-NESs attached using the open-source MoorDyn library, which is widely adopted for simulating dynamic marine structures. This simulation framework allowed us to capture the complex interactions between the subsea cable and external environmental forces, such as tidal currents and platform motions. Multiple B-NESs were attached to the cable, and our formulation facilitated accurate replication of the B-NESs' nonlinear dynamical behaviors by directly mapping their physical characteristics to simulation parameters within the MoorDyn software.

To ensure the validity and robustness of our models, we performed a thorough analytical and numerical study. The analytical results provided a baseline for understanding the fundamental dynamics of the integrated cable/B-NES system, while numerical simulations confirmed the accuracy of our model's predictions. This dual validation approach strengthened the credibility of our findings, ensuring that the model effectively captured the intricate mechanical interactions involved in subsea dynamic power cable stabilization.

The study leveraged a HPC to conduct extensive parametric studies and optimizations, exploring a wide parameter space for the B-NES configurations. Specifically, we considered a vertical subsea baseline cable with four B-NESs attached at strategic locations, subject to prescribed multi-harmonic platform motion at very low frequencies typical of sea wave excitation. By running 2000 discrete simulations on the University of Illinois Urbana-Champaign HPC cluster, we were able to optimize the system parameters of the B-NESs to maximize vibration mitigation across a broad frequency range. Using HPC for this computationally intensive process enabled us to efficiently explore multiple B-NES design variations and identify optimal configurations that would not be feasible using traditional methods.

Our optimization framework demonstrated that the B-NESs can adapt to the non-stationary and broadband vibrational inputs that are typical in subsea environments, a capability that allowed them to outperform traditional (linear) TMDs. Indeed, unlike TMDs, which are limited by their narrowband resonance properties and require precise tuning, the B-NESs demonstrated their unique capacity to dynamically adjust their resonance to frequency shifts, providing effective, broadspectrum energy absorption and mitigation without the risk of amplifying oscillations outside a narrow frequency range (in contrast to TMDs). What enables this ability is the strong (non-linearizable) stiffness nonlinearity of B-NESs, which yields a variable resonance frequency that passively adapts with the changing excitation. This means that, in contrast to the TMD, which has a predetermined resonance frequency, the B-NES is capable of resonating and absorbing energy of cable vibrations with continuously changing frequency and intensity. Moreover, "jumps" in the B-NES transient dynamics due to bi-stability (i.e., jumping back and forth between two stable equilibrium positions) contribute even more to the mitigation efficacy, as the B-NESs act as rapid "scatterers" of vibration energy from lower to higher frequencies within the cable itself. This scattering yields rapid attenuation and dissipation of cable vibrations in a robust way that simply is unattainable with current linear passive mitigating devices.

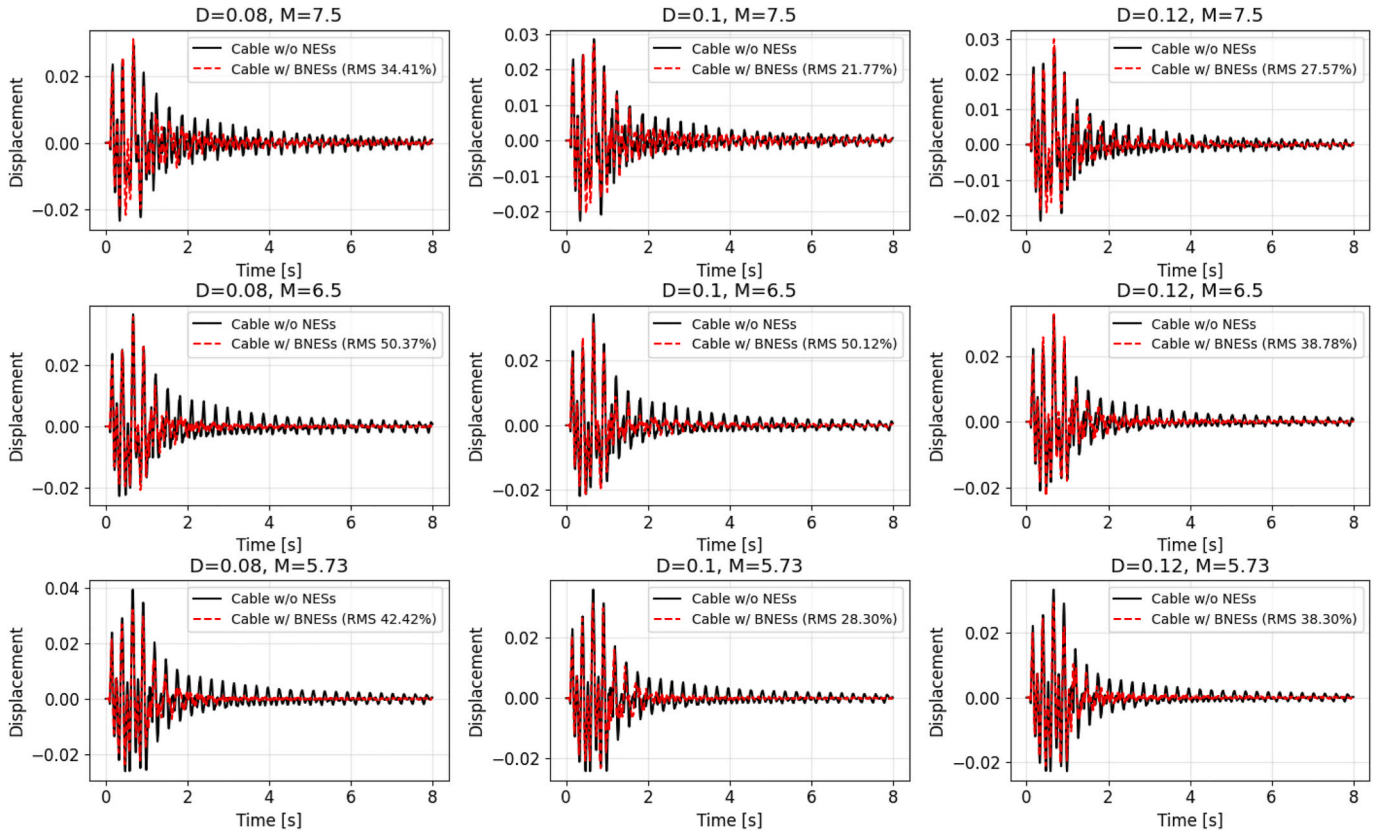

Fig. 14. Transient displacement (in m) at node 5 (at a depth 20.2996 m; see Fig. 2c) of the subsea cable for the cases with and without optimized B-NESs attached; different combinations of cable diameter (D) and mass density (M) are considered (corresponding to the FFT plots of Fig. 13) representing biofouling scenarios.

Our robustness analysis introduced stochastic excitations to capture real-world uncertainties and accounted for variations in the cable's dynamic properties induced by environmental factors such as biofouling. Despite these shifts in the cable's resonant frequencies, the B-NES consistently maintained significant vibration suppression. This outcome further validates the B-NES's broadband capabilities and underscores its potential as a reliable solution for real-world dynamic subsea power cable applications, where environmental and operational conditions are inherently variable.

Although this study successfully demonstrates the effectiveness of a bistable nonlinear energy sink (B-NES) in mitigating vibrations of dynamic subsea power cables through numerical simulations, certain limitations and avenues for further exploration remain. First, structural fatigue resulting from repeated cyclic loading is critical, and further research should quantify fatigue life to highlight the long-term effectiveness of the B-NES. Second, additional complexity—such as torsional dynamics and multidirectional ocean currents—could be introduced to enhance the robustness and realism of the modelling approach. Diverse marine environments should also be investigated to further validate and generalize the proposed solution. Third, further considerations such as installation constraints, maintenance accessibility, and cost may further influence the final number and positioning of B-NES devices. Despite these considerations, the current study lays a foundational framework, providing clear selection criteria and optimization methodologies, which can serve as a robust basis for developing adaptive or reconfigurable B-NES designs applicable across various subsea cable configurations and offshore conditions.

In summary, this study has established the B-NES as a promising passive vibration mitigating device, which, despite its relatively simple configuration, is capable of efficiently and robustly addressing the challenges of vibration mitigation in subsea cable dynamics. This technology, in turn, has the potential to significantly prolong the operational life of cables by reducing the vibration-induced stresses that lead to fatigue and wear. Hence, our findings indicate that B-NESs offer a feasible and impactful retrofit option for enhancing the resilience and stability of existing subsea power infrastructure in offshore wind farms.

Regarding our further considerations on this topic, our future work will focus on demonstrating the efficacy of the B-NES to mitigate VIVs of subsea dynamic power cables, which is a critical factor for their long-term stability, durability, and performance. During the initial implementation of the B-NES within the MoorDyn framework, we considered inline rod elements as attachment points for the B-NES device. Comparisons with baseline cases of the cable—with and without these rods—indicated no significant differences in the overall response. Future work will include additional considerations for the numerical implementation of the B-NES, including further optimization and retrofitting scenarios tailored to different cable designs. Incorporating VIV modeling within the MoorDyn framework will allow us to simulate a broader range of environmental interactions, bringing us closer to a comprehensive solution for reliable and robust subsea cable passive vibration mitigation. To this end, we aim to design and optimize B-NESs for mitigating VIVs of subsea cables, enabling the deployment of these devices in real-world applications. Ultimately, the presented research lays the groundwork for a robust, adaptable, and effective vibration mitigation solution that is cost-effective and has the capacity to drastically improve the reliability, performance, and lifespan of subsea dynamic power cables, making it a valuable contribution to the field of offshore wind energy infrastructure.

CRediT authorship contribution statement

Anargyros Michaloliakos: Writing – review & editing, Writing – original draft, Visualization, Validation, Software, Resources, Project administration, Methodology, Investigation, Formal analysis, Data

curation, Conceptualization. **Wei-Ying Wong:** Writing – review & editing, Writing – original draft, Validation, Supervision, Software, Project administration, Methodology, Investigation, Formal analysis, Data curation. **Ryan Davies:** Writing – review & editing, Writing – original draft, Visualization, Validation, Software, Resources, Methodology, Investigation, Formal analysis, Data curation. **Malakonda Reddy Lekkala:** Writing – review & editing, Validation, Software, Investigation. **Matthew Hall:** Writing – review & editing, Validation, Supervision, Software, Project administration, Methodology, Investigation, Funding acquisition, Formal analysis, Conceptualization. **Lei Zuo:** Writing – review & editing, Supervision, Project administration, Methodology, Investigation, Funding acquisition, Formal analysis, Conceptualization. **Alexander F. Vakakis:** Writing – review & editing, Supervision, Project administration, Methodology, Investigation, Funding acquisition, Formal analysis, Conceptualization.

Declaration of competing interest

The authors declare the following financial interests/personal relationships which may be considered as potential competing interests: The authors report that financial support for this work was provided in part by the National Offshore Wind Research & Development Consortium (NOWRDC).

Acknowledgements

This research was funded in part by the National Offshore Wind Research and Development Consortium (NOWRDC), Contract Ref. No. 187. This support is gratefully acknowledged. The authors also greatly appreciate being granted access to the Hardware-Accelerated Learning (HAL) cluster, which is a High-Performance Computing (HPC) facility at the University of Illinois Urbana-Champaign. This work was authored in part by the National Renewable Energy Laboratory (NREL), operated by the Alliance for Sustainable Energy, LLC, for the U.S. Department of Energy (DOE) under Contract No. DE-AC36-08GO28308. Funding is provided by the U.S. Department of Energy Office of Energy Efficiency and Renewable Energy Wind Energy Technologies Office. The views expressed in the article do not necessarily represent the views of the DOE or the U.S. Government. The U.S. Government retains and the publisher, by accepting the article for publication, acknowledges that the U.S. Government retains a nonexclusive, paid-up, irrevocable, worldwide license to publish or reproduce the published form of this work, or allow others to do so, for U.S. Government purposes.

References

Addison, P.S., 2017. The Illustrated Wavelet Transform Handbook: Introductory Theory and Applications in Science, Engineering, Medicine and Finance. https://doi.org/10.1201/9781315372556. SECOND EDITION, The Illustrated Wavelet Transform Handbook: Introductory Theory and Applications in Science, Engineering, Medicine and Finance, SECOND EDITION.

Assi, G.R.S., Crespi, T., Gharib, M., 2022. Novel geometries of serrated helical strakes to suppress vortex-induced vibrations and reduce drag. Appl. Ocean Res. 120, 103034. https://doi.org/10.1016/J.APOR.2021.103034.

Bellet, R., Cochelin, B., Herzog, P., Mattei, P.O., 2010. Experimental study of targeted energy transfer from an acoustic system to a nonlinear membrane absorber. J. Sound Vib. 329, 2768–2791. https://doi.org/10.1016/J.JSV.2010.01.029.

Drumond, G.P., Pasqualino, I.P., Pinheiro, B.C., Estefen, S.F., 2018. Pipelines, risers and umbilicals failures: a literature review. Ocean Eng. 148, 412–425. https://doi.org/10.1016/J.OCEANENG.2017.11.035.

Elias, S., Matsagar, V., 2017. Research developments in vibration control of structures using passive tuned mass dampers. Annu. Rev. Control 44, 129–156. https://doi.org/10.1016/J.ARCONTROL.2017.09.015.

Fang, Z.-W., Zhang, Y.-W., Li, X., Ding, H., Chen, L.-Q., 2017. Integration of a nonlinear energy sink and a giant magnetostrictive energy harvester. J. Sound Vib. 391, 35–49. https://doi.org/10.1016/j.jsv.2016.12.019.

Frahm, H., 1911. Device for Damping Vibrations of Bodies, 989958.

Gendelman, O.V., 2001. Transition of energy to a nonlinear localized mode in a highly asymmetric system of two oscillators. Nonlinear Dyn. 25, 237–253. https://doi.org/10.1023/A:1012967003477.

Gendelman, O., Manevitch, L.I., Vakakis, A.F., M'Closkey, R., 2001. Energy pumping in nonlinear mechanical oscillators: part I—dynamics of the underlying hamiltonian systems. J. Appl. Mech. 68, 34–41. https://doi.org/10.1115/1.1345524.

Gendelman, O.V., Vakakis, A.F., Bergman, L.A., McFarland, D.M., 2010. Asymptotic analysis of passive nonlinear suppression of aeroelastic instabilities of a rigid wing in subsonic flow. SIAM J. Appl. Math. 70, 1655–1677. https://doi.org/10.1137/090754819.

Gutierrez Soto, M., Adeli, H., 2013. Tuned mass dampers. Arch. Comput. Methods Eng. 20, 419–431. https://doi.org/10.1007/s11831-013-9091-7.

Gzal, M.O., Gendelman, O.V., Bergman, L.A., Vakakis, A.F., 2024. Enhanced seismic mitigation through energy management using nonlinear energy sinks with clearance–contacts. Nonlinear Dyn. https://doi.org/10.1007/s11071-024-10293-8.

Hall, M., 2020. Moordyn v2: new capabilities in mooring system components and load cases. In: Proceedings of the International Conference on Offshore Mechanics and Arctic Engineering - OMAE. https://doi.org/10.1115/omae2020-19341.

Hall, M., Goupee, A., 2015. Validation of a lumped-mass mooring line model with DeepCwind semisubmersible model test data. Ocean Eng. 104, 590–603. https://doi.org/10.1016/J.OCEANENG.2015.05.035.

Hall, M., Housner, S., Sirnivas, S., Wilson, S., 2021. MoorPy (Quasi-Static mooring analysis in python). https://doi.org/10.11578/dc.20210726.1.

Hall, Matthew, Sirnivas, S., Yu, Y.-H., 2021. Implementation and verification of cable bending stiffness in MoorDyn. In: ASME 2021 3rd International Offshore Wind Technical Conference. American Society of Mechanical Engineers. https://doi.org/10.1115/IOWTC2021-3565.

Hoang, N., Fujino, Y., Warnitchai, P., 2008. Optimal tuned mass damper for seismic applications and practical design formulas. Eng. Struct. 30, 707–715. https://doi.org/10.1016/J.ENGSTRUCT.2007.05.007.

Housner, S., Lozon, E., Martin, B., Brefort, D., Hall, M., 2022. Seabed bathymetry and friction modeling in MoorDyn. J. Phys. Conf. https://doi.org/10.1088/1742-6596/2362/1/012018.

Kremer, D., Liu, K., 2014. A nonlinear energy sink with an energy harvester: transient responses. J. Sound Vib. 333, 4859–4880. https://doi.org/10.1016/J.JSV.2014.05.010.

LLOYD Warwick, 2021. International offshore wind loss adjusters perspective [WWW Document]. ORE Catapult. URL. https://www.dnv.com/article/80-percent-of-insurance-claims-in-offshore-wind-are-related-to-subsea-cable-failures-how-can-the-industry-manage-these-risks/, 12.1.24.

Manevitch, L.I., Sigalov, G., Romeo, F., Bergman, L.A., Vakakis, A., 2014. Dynamics of a linear oscillator coupled to a bistable light attachment: analytical study. Journal of Applied Mechanics, Transactions ASME 81. https://doi.org/10.1115/1.4025150.

Mann, B.P., Sims, N.D., 2009. Energy harvesting from the nonlinear oscillations of magnetic levitation. J. Sound Vib. 319, 515–530. https://doi.org/10.1016/J.JSV.2008.06.011.

Marty, A., Berhault, C., Damblans, G., Facq, J.V., Gaurier, B., Germain, G., Soulard, T., Schoefs, F., 2021. Experimental study of hard marine growth effect on the hydrodynamical behaviour of a submarine cable. Appl. Ocean Res. 114, 102810. https://doi.org/10.1016/J.APOR.2021.102810.

Michaloliakos, A., Wang, C., Vakakis, A.F., 2023. Machine learning extreme acoustic non-reciprocity in a linear waveguide with multiple nonlinear asymmetric gates. Nonlinear Dyn. 111, 17277–17297. https://doi.org/10.1007/s11071-023-08765-4.

Miranda, J.C., 2005. On tuned mass dampers for reducing the seismic response of structures. Earthq. Eng. Struct. Dynam. 34, 847–865. https://doi.org/10.1002/eqe.461.

Mojahed, A., Moore, K., Bergman, L.A., Vakakis, A.F., 2018. Strong geometric softening–hardening nonlinearities in an oscillator composed of linear stiffness and damping elements. Int. J. Non Lin. Mech. 107. https://doi.org/10.1016/j.ijnonlinmec.2018.09.004.

Nili Ahmadabadi, Z., Khadem, S.E., 2014. Nonlinear vibration control and energy harvesting of a beam using a nonlinear energy sink and a piezoelectric device. J. Sound Vib. 333, 4444–4457. https://doi.org/10.1016/J.JSV.2014.04.033.

Nucera, F., McFarland, D.M., Bergman, L.A., Vakakis, A.F., 2010. Application of broadband nonlinear targeted energy transfers for seismic mitigation of a shear frame: computational results. J. Sound Vib. 329, 2973–2994. https://doi.org/10.1016/J.JSV.2010.01.020.

Ormondroyd, J., Den Hartog, J.P., 1928. The theory of the dynamic vibration absorber. Trans. ASME J. Appl. Mech. 50, 9–22.

Quen, L.K., Abu, A., Kato, N., Muhamad, P., Sahekhaini, A., Abdullah, H., 2014. Investigation on the effectiveness of helical strakes in suppressing VIV of flexible riser. Appl. Ocean Res. 44, 82–91. https://doi.org/10.1016/J.APOR.2013.11.006.

Quinn, D.D., Triplett, A.L., Bergman, L.A., Vakakis, A.F., 2011. Comparing linear and essentially nonlinear vibration-based energy harvesting. J. Vib. Acoust. 133. https://doi.org/10.1115/1.4002782.

Rana, R., Soong, T.T., 1998. Parametric study and simplified design of tuned mass dampers. Eng. Struct. 20, 193–204. https://doi.org/10.1016/S0141-0296(97)00078-3.

Remick, K., Dane Quinn, D., Michael McFarland, D., Bergman, L., Vakakis, A., 2016. High-frequency vibration energy harvesting from impulsive excitation utilizing intentional dynamic instability caused by strong nonlinearity. J. Sound Vib. 370, 259–279. https://doi.org/10.1016/J.JSV.2016.01.051.

Romeo, F., Sigalov, G., Bergman, L.A., Vakakis, A.F., 2015. Dynamics of a linear oscillator coupled to a bistable light attachment: numerical study. J. Comput. Nonlinear Dynam. 10. https://doi.org/10.1115/1.4027224.

Sardar, R., Chakraborty, S., 2025. Wave vibration mitigation of offshore structures using a compliant cell tuned liquid mass damper. Ocean Eng. 327, 120994. https://doi.org/10.1016/J.OCEANENG.2025.120994.

Skopljak, N., 2016. GCube: most financial losses are Down to the subsea wire [WWW Document]. Offshore Wind. URL. https://www.offshorewind.biz/2016/06/15/gcube-most-financial-losses-are-down-to-the-subsea-wire/, 12.1.24.

Starosvetsky, Y., Gendelman, O.V., 2010. Interaction of nonlinear energy sink with a two degrees of freedom linear system: internal resonance. J. Sound Vib. 329, 1836–1852. https://doi.org/10.1016/J.JSV.2009.11.025.

Strang-Moran, C., 2020. Subsea Cable Management: Failure Trending for Offshore Wind. Wind Energy Science Discussions, p. 2020. https://doi.org/10.5194/wes-2020-56.

Tian, H., Soltani, M.N., Nielsen, M.E., 2023. Review of floating wind turbine damping technology. Ocean Eng. 278, 114365. https://doi.org/10.1016/J.OCEANENG.2023.114365.

Tsai, H.C., 1995. The effect of tuned-mass dampers on the seismic response of base-isolated structures. Int. J. Solid Struct. 32, 1195–1210. https://doi.org/10.1016/0020-7683(94)00150-U.

Vakakis, A.F., Gendelman, O., 2001. Energy pumping in nonlinear mechanical oscillators: part II—Resonance capture. J. Appl. Mech. 68, 42–48. https://doi.org/10.1115/1.1345525.

Vakakis, A., Gendelman, O.V., Bergman, L.A., McFarland, D.M., Kerschen, G., Lee, Y.S., 2009. Nonlinear targeted energy transfer in discrete linear oscillators with Single-DOF nonlinear energy sinks. In: Nonlinear Targeted Energy Transfer in Mechanical and Structural Systems. Springer, Netherlands, Dordrecht, pp. 93–302. https://doi.org/10.1007/978-1-4020-9130-8_3.

Vakakis, A.F., Gendelman, O.V., Bergman, L.A., Mojahed, A., Gzal, M., 2022. Nonlinear targeted energy transfer: state of the art and new perspectives. Nonlinear Dyn. 108, 711–741. https://doi.org/10.1007/s11071-022-07216-w.

Wang, J., Li, H., Zhang, J., Guan, D., Lin, X., Chen, H., 2025. Experimental investigations in the effect of passive gyro stabilizers on the pitch motion of a semi-submersible floating wind turbine. Ocean Eng. 321, 120403. https://doi.org/10.1016/J.OCEANENG.2025.120403.

Wierschem, N.E., Luo, J., Hubbard, S., Fahnestock, L.A., Spencer Jr., B.F., Vakakis, A.F., Bergman, L.A., 2013. Experimental testing of a large 9-Story structure equipped with multiple nonlinear energy sinks subjected to an impulsive loading. In: Structures Congress 2013. American Society of Civil Engineers, Reston, VA, pp. 2241–2252. https://doi.org/10.1061/9780784412848.196.

Zhang, Y., Tang, L., Liu, K., 2017. Piezoelectric energy harvesting with a nonlinear energy sink. J. Intell. Mater. Syst. Struct. 28, 307–322. https://doi.org/10.1177/1045389X16642301.

Zheng, H., Wang, J., 2017. Numerical study of galloping oscillation of a two-dimensional circular cylinder attached with fixed fairing device. Ocean Eng. 130, 274–283. https://doi.org/10.1016/J.OCEANENG.2016.11.074.